NTNU
Norwegian University of
Science and Technology

Complex behaviors of clay particles in air and CO2

Mohsen Dahesh

Condensed Matter Physics
Submission date: July 2011
Supervisor: Jon Otto Fossum, IFY

Norwegian University of Science and Technology
Department of Physics

Faculty of Natural Science and Technology
Department of Physics

MASTER'S THESIS FOR

Mohsen Dahesh

Thesis started: 15. January 2010
Thesis submitted: 31. July 2011

DISCIPLINE: CONDENSED MATTER PHYSICS

Title: *Complex behaviors of clay particles in air and* CO_2

This work has been carried out at the Complex Materials Division at Department of Physics NTNU, under the supervision of Professor Jon Otto Fossum

---

Trondheim, 31. July 2010

Jon Otto Fossum

Responsible supervisor

Professor at Department of Physics

To My Mother

ABSTRACT

Part I

The shear rheology of nano-clay particles when dispersed in liquid CO_2 under elevated pressure using the Couette geometry is studied. A high pressure attachment with two different measuring systems - the double gap and Mooney systems - is used for this purpose. The clays are Laponite, Quick clay, Na-fluorohectorite and Na-montmorillonite. The shear viscosities of the dispersions are measured under increasing shear rates or shear stresses. In addition an ageing test is carried out for six days for a laponite-liquid CO_2 dispersion. Inertia of the system is compensated for by control shear stress tests.

Part II

E-field induced chain formations of the nano-clay particles when dispersed in the air are recorded by a camera. A glove bag is prepared in such a way as to provide a Nitrogen atmosphere and the procedure is repeated in this glove bag. In both situations the chain formations are observed. An attempt to measure the leakage of current within the electrode is also made by means of an operational amplifier and feedback resistor, even though the measurement of the current is uncertain.

ACKNOWLEDGMENTS

I would like to thank firstly my supervisor Professor Jon Otto Fossum for his help and advice. I am also thankful for the assistance of all the members of the Laboratory of soft and complex matter studies at NTNU, especially PhD student Henrik Hemman and Zbigniew Rozynek and Pos.doc candidate Dr.Davi de Miranda Fonseca and technician Ole Tore Buset. I would not have been able to finish my experiments on time without their help. I feel the need to thank Master students Mohammad Hanif, Gotfrid Inkoom, Kofi Tutu Addo Assuming-Gyimah and Erlend Granbo Rolseth for their fruitful discussions, and Andrew Fleming for his help with English grammar. To my family and friends, I thank you for always being there for me and for understanding when I was not always attentive to spending time with you. Finally, I thank the Lord for blessing me with gifts of scientific curiosity and understanding as well as for good health and fortune.

Mohsen Dahesh
Trondhiem, July 2011

Contents

ABSTRACT iii

ACKNOWLEDGMENT iv

I Complex behavior of clay particles in carbon dioxide (High pressure rheology Of Nano-clays suspended in liquid carbon dioxide) 1

1 Introduction 3

2 Theory 5
2.1 Clays 5
2.2 Carbon Dioxide 12
2.3 Rheology 14
2.4 Particulate suspension 24

3 Experiment 25
3.1 Experimental set up 25
3.2 Experimental method 32

4 Data analysis and results 35
4.1 Checking of the friction of the ball bearing 35

4.2 Rheology of clay and CO_2 in the double gap system DG35.12/PR 36
4.3 Rheology of clay and CO_2 in the coaxial cylinder system CC33.2/PR 45
4.4 Discussion 48

5 Conclusions and suggestions for future studies 63

II Complex behavior of clay particles in air (Imaging of E-Field induced chain formation from Nano-clays in air) 65

6 Introduction 67

7 Theory 69
7.1 Electrorheological models 69
7.2 The Simple polarization model 71

8 Experiment 75
8.1 Experiment set up 75
8.2 Material 77

9 Data Analysis and results 79
9.1 Imaging of clay particles in ambient atmosphere 79
9.2 Imaging of clay particles in Nitrogen atmosphere 83
9.3 Discussion 83

10 Conclusions and suggestions for future studies 91

LIST OF FIGURES 97

References 97

Part I

Complex behavior of clay particles in carbon dioxide (High pressure rheology Of Nano-clays suspended in liquid carbon dioxide)

Chapter 1

Introduction

Clay minerals are of great importance in soil science, carbon dioxide storage and natural gas and petroleum reservoir engineering. They are a porous media and a role of their formation in gas or oil reservoirs is to trap the buoyant fluid in a lower porous formation [1]. Penetration of fluids in porous systems has been extensively studied, including water penetration in clay caprock which causes clay to swell. The same is true if clay material is poorly consolidated. Fluids like carbon dioxide are injected into deep saline aquifers and hydrocarbon reservoirs for many purposes, such as enhancing oil recovery and recently for carbon dioxide storage. Carbon dioxide storage involves the capture and injection of CO_2 into a deep surface formation offering one solution to the problem of the atmospheric emissions of greenhouse gases. The CO_2 will have a sufficiently high pressure and temperature to be in a supercritical state. The density of injected carbon dioxide will be higher than that of its gaseous state [2]. To study carbon dioxide flow behavior in conditions which are the same as deep surfaces, high pressure tools are applied. One of these tools is a high pressure cell mounted in a viscometer (Rheometer) which measures viscosity, among other things, under high pressure. The term rheology refers to the study of deformation and flow of matter [3]. in the case of high pressures or temperatures, high pressure rheology is the study of

flow behavior under elevated pressures. Systems like clay-water show interesting rheological properties. They are called colloidal suspensions which are plate-like clay particles suspended in water. Structures which form in these systems are large scaled in length compared to molecular dimensions which can lead to interactions between the flow field and the organization of the fluid. Such interaction is shear thinning where viscosity decreases strongly with shear rate. Viscosity also is dependent on pressure and temperature and can vary exponentially with them. In this work the system is clay-liquid CO_2. We are trying to measure the viscosity and flow curve of clays dispersed in the liquid CO_2 at a pressure of 60 bar and temperature of 10°C. Different types of clays used include Laponite, Quick clay, Na-Montmorillonite and Na-Fluorohectorite. This work is new in the laboratory of soft matter physics at NTNU, and we are expected as new students to continue this work in systems like clay-water-CO_2 which resembles the conditions at deep surfaces. The first part of this thesis inlcudes five chapters. Chapter one discusses theory, chapter two gives the experiment setup and method, chapter three provides data analysis and chapter five discusses conclusions and suggestions for future work.

Chapter 2

Theory

2.1 Clays

The term clay is used in several senses. It is a term for a rock implying a natural, earthy, fine-grained material that develops plasticity when mixed with a limited quantity of water. It is also a term for a particle, long used in the analysis of sedimentary rocks and soils, associated with an upper particle size of 2 μm. This limit corresponds to a natural break between clay minerals, which normally exist as particles of < 2 μm, and non-clay minerals which occur above this size. The clay mineral concept advanced in the 1920s and 1930s-that the clay fraction of a soil or rock consists of small particles of a limited number of crystalline materials-was substantiated over the period from about 1930 to 1960. Clay minerals in their large volume state are exploited as unreactive fillers in polymers, paints, or the paper industry, their value arising from substitution for other more expensive materials or from physical function-ality (arising from the anisotropic particle shape). However, clay minerals are also chemically reactive. Their use in ceramics, for example, follows from phase changes and intercrystal reactivity. Finally, although clays are usually natural, they can be made synthetically, with specific ionic substitutional patterns.Such materials find use, for example, as

rheology modifiers [4].

2.1.1 Structures

All clay minerals have structures based on silica tetrahedrons linked via corner sharing into two-dimensional ribbons or sheets. The other major structural elements-alumina or magnesia octahedrons-are joined to the tetrahedrons through shared oxygen atoms. This is illustrated in Figure 2.1 and 2.2.

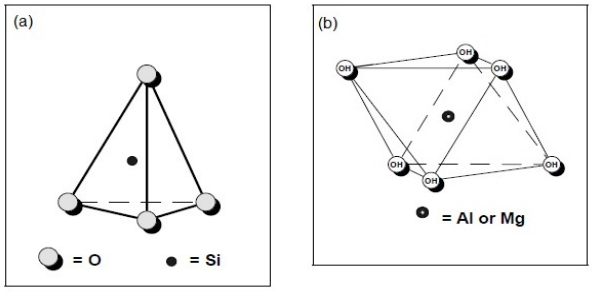

FIGURE 2.1: (a) Tetrahedron (b) Octahadron [5].

Three major classes of clay minerals exist: Two are layered, while one is based on chains or ribbons. Layer silicates are either of the 1:1 or T:O type, typified by kaolinite (one tetrahedral sheet joined to one octahedral sheet), or 2:l or smectite or T:O:T type typified by muscovite (Fig 2.3) [4, 6].
Layer silicates of either of these classes can be either dioctahedral or trioctahedral, depending upon whether two-thirds of all the octahedral sites or all of them are filled (which depends on the octahedral cation charge). The third class, based on chains or ribbons, contains the minerals sepiolite and paly-gorskite. In both cases the ribbons consist of 2:l or T:O:T structures, but they differ in ribbon sizes. Ribbons are joined to adjacent ones through oxygen atoms shared between adjacent tetrahedrons. The layers in 1:1 clay mineral are only held together by weak forces (van der Waals and, possibly, hydrogen bonding) while those in 2:l minerals are attracted electrostatically, the extent being related to the layer charge. In

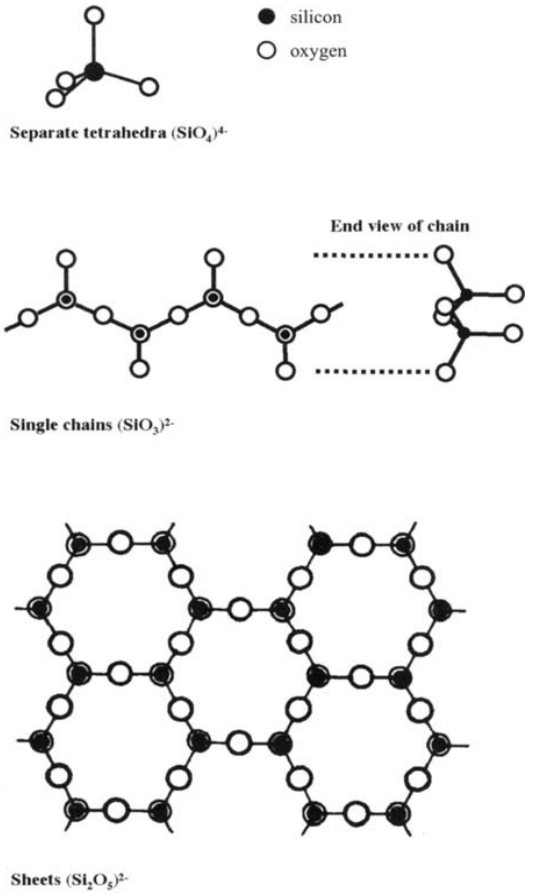

FIGURE 2.2: Silicate building blocks [4].

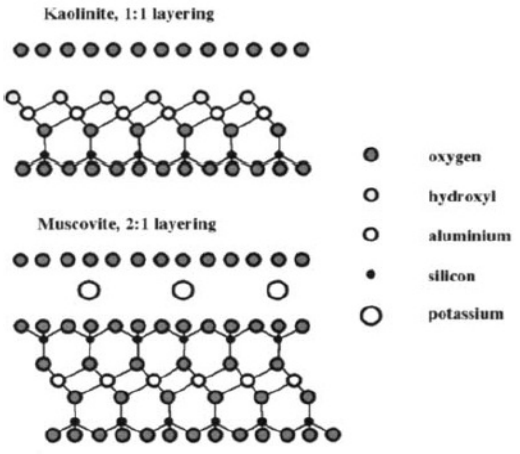

FIGURE 2.3: Up:1:l(T:O) Kaolinite and Down 2:l (T:O:T) muscovite [4].

both cases, guest species can intercalate between the layers. Ribbon-based mineral structures are stable in three dimensions (at room temperature and pressure) but guest species can intrude into the space between the ribbons [4].

2.1.2 Water-swellable clay

Water-swellable Clays are mineral based. Most are produced from clay minerals of the smectite group of clays, principally hectorite and bentonite. When dispersed in water (not dissolved, for they are not soluble in water), the clay particles do swell (hence the name) and, if exposed to sufficient shear forces during mixing, separate into individual clay platelets. Because these platelets have negatively-charged faces and edges with a small positive charge, the edges of one platelet are attracted to the faces of another platelet and they develop a three-dimensional, 'house-of-cards' colloidal structure. This colloidal structure provides thickening and other desirable rheological effects [7].

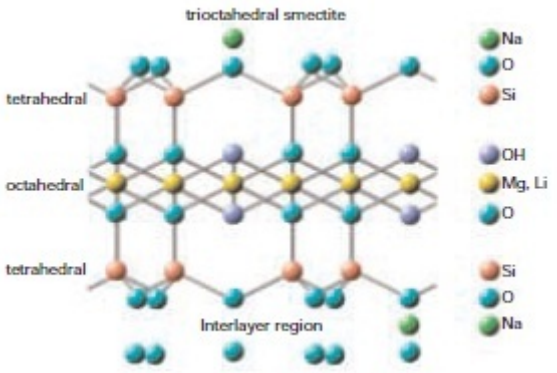

FIGURE 2.4: Idealised structural formula of Laponite [8].

Laponite

Laponite is a synthetic, layered silicate that resembles the natural smectite mineral-hectorite in both structure and composition. Its unique properties are related to the primary platelet size of laponite, which is only 25 nm across and 1 nm thick, significantly smaller than the naturally occurring materials. The idealized structure shown in figure 2.4 would have a neutral charge with six divalent magnesium ions in the octahedral layer, giving a positive charge of twelve. In practice, however, some magnesium ions are substituted by lithium ions (monovalent) and some positions are empty to give a composition which typically has the empirical formula:

$$\mathrm{Na}^{+}_{0.7}[(\mathrm{Si}_8\mathrm{Mg}_{5.5}\mathrm{Li}_{0.3})\mathrm{O}_{20}(\mathrm{OH})_4]^{-0.7} \tag{2.1}$$

The crystals become arranged into stacks which are held together electrostatically by sharing of sodium ions in the interlayer region between adjacent crystals [8].

Kaolinite

Kaolinite particles consist of alumino silicate layers, responsible for their plate-shaped geometry. The layers are held together by hydrogen bonding between hydroxyls from the alumina sheet on one face and oxygens from the silica sheet on the opposite face. These forces are relatively strong, preventing hydration between layers and allowing many layers to build up. The ideal formula of kaolinite is

$$\mathrm{Al_2Si_2O_5(OH)_4} \tag{2.2}$$

Its structure type is 1:1 or T:O with an average diameter of kaolinite particles of 0.32μm. Most of the cation exchange capacity of kaolinite can be attributed to the dissociation of OH groups on clay edges. The charge on the faces of the kaolin particles is negative and pH independent, while the charge on the edges changes from positive to negative values with increasing pH, due to the coexistence of both positive and negative charges. Between pH 5 and 9, the edge surface is expected to be negatively charged. Kaolinite is a coarse clay with low colloidal activity, that is, low plasticity and cohesion, and low swelling and shrinkage [9, 10].

Na-Fluorohectorite

Fluorohectorite clay was produced by Corning, and ion exchanged through dialysis to produce Na-Fluorohectorite having the nominal chemical formula

$$\mathrm{Na_{0.6}[(Mg_{2.4}Li_{0.6}Si_4)O_{10}F_2]} \tag{2.3}$$

whose two inverted silicate tetrahedral layers share their apical oxygens with one octahedral layer [11]. Na-Fluorohectorite(Na-Fh) has a structure type of 2:1 or T:O:T and is a swelling clay that incorporates a variable amount of water in the interlayer space, resulting in a change in lattice constant along the stacking direction. It also has a quite large and variable particle size of up to 2μm in diameter [12]. In figure 2.5 the atomic structure of Na-Fluorohectorite is shown.

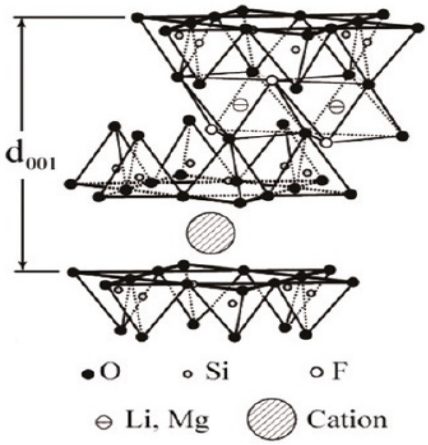

FIGURE 2.5: Na-Fluorohectorite with T:O:T structure, Na^+ is intercalated cation [13].

Na-Montmorillonite

Na-Montmorillonite was produced in Wyoming. Montmorillonite is the main component of dry betonite, and is built up by two tetrahedral and one octahedral unit forming a platelet approximately 10 nm thick. Na-Montmorillonite with a typical unit formula

$$Na_x[(Al_{2-x}Mg_x)Si_40_{10}(OH)_2] \tag{2.4}$$

has a structure type of 2:1 or T:O:T and is a swelling clay. The platelets form a lamellar structure making betonite or Montmorillonite clay, a seemingly perfect model system for an electrical double layer where the swelling and stability in saline solution depend strongly on counterion valency and surface charge density [9, 14].

Quick Clay

The composition of the Quick clay, collected from about 10 m depth at Tiller, Trondheim, as determined by x-ray diffraction, is 70 wt% non-swelling clays (illite, chlorite, and some kaolinite) and a few percent swelling clays (vermiculite and montmorillonite). Texture analysis of the Quick clay shows that the particles are plate like and very fine [15].

2.2 Carbon Dioxide

Carbon dioxide with a chemical formula CO_2 is a chemical compound composed of two oxygen atoms covalently bonded to a single carbon atom, with a linear molecule, a bond angle 180^{o} and zero net dipole moment. Carbon dioxide is a colorless, odorless and tasteless gas and 1.53 times heavier than air. It has a density of 1.80 $\mathrm{kg/m^3}$ at $25^{o}\mathrm{C}$ and can be liquefied under pressure. It liquefies at $-56.6^{o}\mathrm{C}$ at 5.2 atm at triple point. The density of liquid CO_2 at $0^{o}\mathrm{C}$ and 34 atm is 914 $\mathrm{kg/m^3}$. It also solidifies to white snow-like flakes known as dry ice, at a density of 1560 $\mathrm{kg/m^3}$ at $-79^{o}\mathrm{C}$. Carbon dioxide‘s critical temperature and critical pressure are $31.1^{o}\mathrm{C}$ and 72.79 atm respectively. It is moderately soluble in water - its solubility is 173mL and 88mL $CO_2/100$ mL water at $0^{o}\mathrm{C}$ and $20^{o}\mathrm{C}$ respectively, and its solubility increases with pressure [16]. The phase diagram of carbon dioxide is shown in figure 2.6.

2.2.1 Liquid and supercritical carbon dioxide

Liquid carbon dioxide is usually stored under 20 bar pressure at $-18^{o}\mathrm{C}$. Compression and cooling of the gas between the temperature limits at the ‘triple point’ and the ‘critical point’ will cause it to liquefy. The triple point is the pressure temperature combination at which carbon dioxide can exist simultaneously as gas, liquid and solid. Above the critical temperature point of $31^{o}\mathrm{C}$ it is impossible to liquefy the gas by increasing the pressure above the critical pressure of 73 bar.

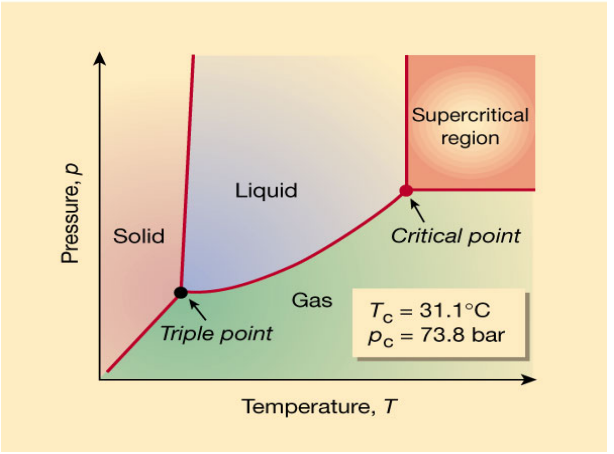

FIGURE 2.6: Phase diagram for carbon dioxide [17].

Reduction in the temperature and pressure of liquid below the triple point causes the liquid to disappear, leaving only gas and solid. Liquid carbon dioxide produces a colorless, dense, non-flammable vapor with a slightly pungent odor and characteristic acid 'taste' [18]. Carbon dioxide above its critical point becomes supercritical. A substance above its critical temperature and critical pressure is considered to be a supercritical fluid. The critical point represents the highest temperature and pressure at which the vapor and liquid phase of a substance can co-exist in equilibrium. Above the critical point, the distinction between gas and liquid does not apply and the substance can only be described as a fluid. The physical properties of supercritical CO_2, such as, density, viscosity and diffusivity coefficient can be varied between the limits of gas and near liquid properties by controlling temperature and pressure. Figure 2.7 illustrates the phase change of CO_2 from distinct gas and liquid phases to a homogeneous supercritical phase [19]. At supercritical conditions, carbon dioxide has a density similar to a liquid and viscosity and diffusivity comparable to a gas [20].

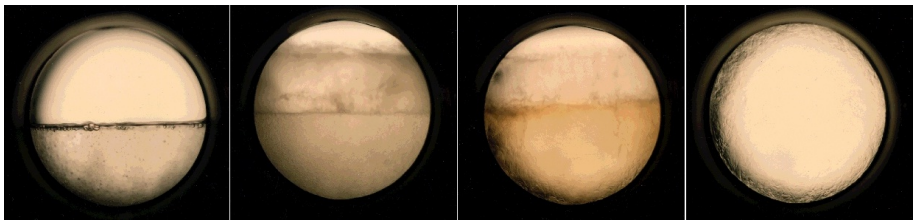

FIGURE 2.7: A chamber containing two phases of carbon dioxide–liquid and gas. As temperature and pressure increase (from left to right), the two phases merge to become a supercritical fluid [19]

2.3 Rheology

Rheology has been properly defined as the study of the flow and deformation of materials. In flow, elements of the liquid are deforming, and adjacent points in the liquid are moving relative to one another. There are two basic kinds of flow with relative movement of adjacent particles of a liquid: Shear and extensional flows. In shear flows liquid elements flow over or past each other, while in extensional flow, adjacent elements flow towards or away from each other. See figure 2.8 for illustrations of shear and extensional deformation and flow, respectively [21].

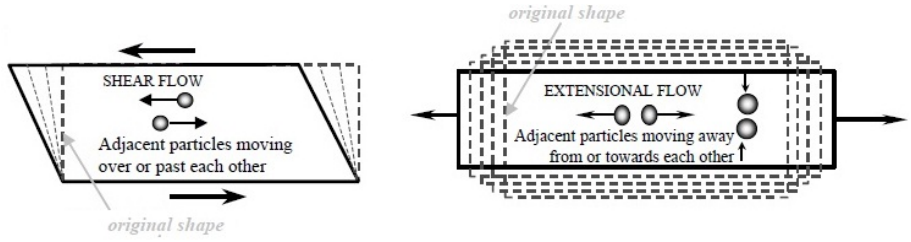

FIGURE 2.8: Particle motion in shear and extensional flow [21].

2.3.1 Definitions

Stress and Strain: *Stress* is simply defined as the force divided by the area over which it is applied.

$$\sigma = \frac{F}{A} \tag{2.5}$$

When a stress is applied to a material, a deformation will occur. Strain is defined as relative deformation, i.e. deformation per unit length. In figure 2.9 (left) tensile stress and strain are shown. At small stress and strain, the stress is directionally proportional to the strain, and proportionality constant - Young's Modulus - and this linearity is expressed by Hook's law.

$$\sigma = Y\epsilon \tag{2.6}$$

In figure 2.9 (right) shear stress is illustrated, for a Hookean solid. Shear stress applied to the surface as shown in the figure 2.9, results in an instantaneous deformation. Once the deformed state is reached, there is no further movement, but the deformed state persists as long as the stress is applied. The angle α is referred to as the strain γ and the relevant constitutive equation is

$$\sigma = G\gamma \tag{2.7}$$

where G is referred to as the shear modulus.

Shear rate and flow: Consider two surfaces separated by a small gap containing a liquid, as illustrated in figure 2.10. A constant shear stress must be maintained on the upper surface for it to move at constant velocity, *u*. With the assumption that there is no slip between the surface and the liquid, there is a continuous change in velocity across the small gap to zero at lower surface. Now in each second the displacement produced is *x* and the strain is

$$\gamma = \frac{x}{z} \tag{2.8}$$

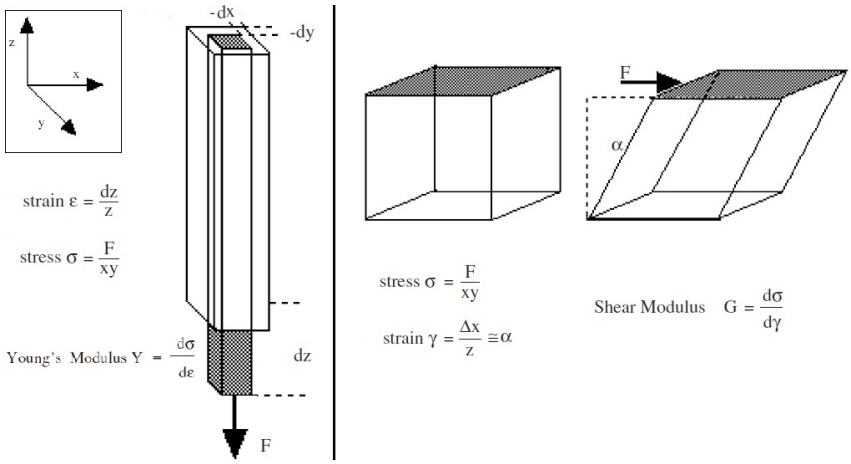

FIGURE 2.9: Left tensile stress and right shear stress [22]

and as $\mathrm{u} = \frac{\mathrm{dx}}{\mathrm{dt}}$, we can write the rate of strain as

$$\frac{d\gamma}{dt} = \frac{u}{z} \tag{2.9}$$

The rate of strain or shear rate with Newtons dot indicates the differential operator with respect to time. For large gaps the shear rate will vary across the gap and we would find

$$\dot{\gamma} = \frac{du}{dz} \tag{2.10}$$

A shear stress σ results in flow. In the case of a Newtonian liquid, the flow persists as long as the stress is applied. The shear stress σ is proportional to the shear rate $\dot{\gamma}$. The constant of proportionality η is viscosity coefficient [3, 22].

$$\sigma = \eta\dot{\gamma} \tag{2.11}$$

All flows are resisted by viscosity. Liquids are made to flow by imparting a ve-

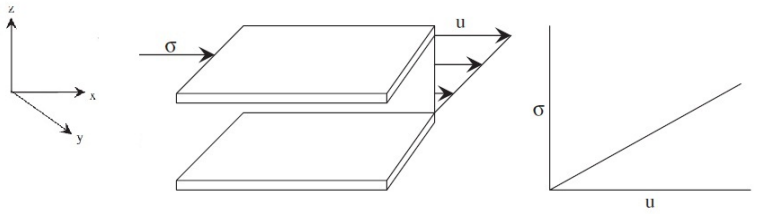

FIGURE 2.10: A velocity gradient produced when a fluid is sheared [22].

locity as in stirring with a spoon, or else by applying a force, as with squeezing a bottle of sauce. For a given velocity the resulting force increases when the viscosity is increased, whereas for a given force, the velocity is reduced when the viscosity is increased [21]. Simple forms of rheological behavior are

$$\text{for a Hookean solid} \quad \sigma = G\gamma \tag{2.12}$$

$$\text{and a Newtonian liquid} \quad \sigma = \eta\dot{\gamma} \tag{2.13}$$

These equations describe linear behavior which is limited. Usually large stresses and strains or short times cause deviations from equations 2.12 or 2.13 which show nonlinear behavior [22].

2.3.2 High pressure rheology

High-pressure rheological experiments generally apply the same experimental techniques that are used in conventional ambient pressure experiments. Thus the most obvious way to design a high pressure rheological experiment is to simplify and miniaturize a conventional rheometer and enclose it within a pressure vessel [23]. Therefore measurements carried out with the pressure vessel can be useful to investigate process conditions such as crude oil production and the pumpability of various dispersions. In fact the pressure vessel is an accessory for the cylinder

temperature and pressure control devices and is fully closed to the environment and it can either be used as a self-pressurizing system or pressurized by using a gas tube or compressor [24, 25].
Generally the viscosity of liquids and most fluids increases exponentially with isotropic pressure, because the amount of free volume in its internal structure decreases due to compression. But the changes are quite small for pressures differing from atmospheric pressure by about one bar. Therefore, for most practical purposes, the pressure effect is ignored by users. However, in certain situations this would not be justified. For example, the oil industry requires measurements of the viscosity of lubricants and drilling fluids at elevated pressures. Rheology under pressure is used to simulate process conditions, to measure above the boiling point of fluids and to prevent sample evaporation [3].
The local pressure-viscosity and temperature-viscosity coefficient, may be defined as

$$\alpha(T,p) = \frac{\partial(\ln \eta_0)}{\partial p} \tag{2.14}$$

$$\beta(T,p) = -\frac{\partial(\ln \eta_0)}{\partial T} \tag{2.15}$$

Where η_0 is the low shear viscosity , then the pressure rate of change of β is

$$\frac{\partial \beta}{\partial p} = -\frac{\partial \alpha}{\partial T} \tag{2.16}$$

At pressures for which α is increasing with pressure, β can become very much larger than its value at ambient pressure [23]. A useful empirical model for the pressure and temperature effect on the limiting low shear rate viscosity is

$$\eta_0 = \kappa e^{ap} e^{bT} \tag{2.17}$$

where κ, a and b are constant. Actually this equation is relatively easy to use in solving flow problems and is valid over a temperature range of about 50K and pressure change of 1 kbar for polymers. A relation that is valid over a wider

temperature range is the Andrade-Eyring equation:

$$\eta_0 = K_2 e^{E_n/RT} \tag{2.18}$$

This equation was derived from the hypothesis that small molecules move by jumping into unoccupied sites or holes. For many small molecule liquids $\mathrm{E}_\eta = 10 - 30\mathrm{KJ/mol}$. Near the glass transition temperature in polymers, E_η decreases. This decrease can be explained by the extra free volume created by thermal expansion, which leads to the Williams-Landel-Ferry (WLF) equation [26]. When flow curves obtained at different temperatures (or pressures) for one material are plotted as $\log \eta$ versus $\log \dot{\gamma}$, the curves have the same shape and the relationships between the variables have the same functional form. The same holds true for $\log \tau$ versus $\log \dot{\gamma}$ or $\log \eta$ versus $\log \tau$. This is a simple form of the useful principle known as time-temperature-pressure superposition or the method of reduced variables [23]. To describe time-temperature superposition and other shifts in viscosity data of certain fluids, free volume equations are normally employed, if we use Doolittle's simple equation:

$$\eta_0 = A e^{B/f} \tag{2.19}$$

where f is the fractional free volume, and A and B are material constant dependent. Fractional free volume is defined by

$$f = \frac{V - V_\Phi}{V} \tag{2.20}$$

where V is the specific volume of the material which is equal to the reciprocal of its mass density and the subscript Φ refers to the occupied volume. The Williams-Landel-Ferry (WLF) equation is an adaptation of the Doolittle equation. The WLF equation assumes linear temperature dependence on fractional free volume from $\mathrm{T_g}$ (Glass transition), to about 100°C + $\mathrm{T_g}$. The WLF equation describes the viscosity at temperature T in terms of viscosity at some reference temperature $\mathrm{T_r}$.

$$\log a_T = \log \frac{\eta(T)}{\eta(T_r)} = \frac{-C_1(T - T_r)}{C_2 + (T - T_r)} \tag{2.21}$$

where C_1 and C_2 are constant and T is temperature and T_r is the reference temperature. If T_g glass transition was linear pressure dependent, $\mathrm{T_{g,p}} = \mathrm{T_{g,p_0}} + \mathrm{A_1 p}$ where A_1 is the rate of change of T_g with pressure and T_{g,p_0} is the glass transition temperature at atmospheric pressure. If we rewrite the equation 2.21 with $\mathrm{T_{g,p}}$, we have

$$\log a_{T,p} = \log \frac{\eta}{\eta_g} = \frac{(A_2 + A_3 p)}{(A_4 - A_1 p)} \tag{2.22}$$

where $A_2 = -c_1(T - T_{gp_0}), A_3 = c_1 A_1, A_4 = c_2 + T - T_{gp_0}$.

2.3.3 Rheometric measurement

Many types of rheometers are available to characterize complex fluid. They can be classified into four categories: Pressure driven, falling bodies, rotational and vibrating devices. Each type has some significant advantages and disadvantages. Pressure-driven devices such as capillary viscometers or slit die viscometers are accurate and provide simple flow fields, but the pressure drop across the capillary can lead to a situation where the properties of the fluid at the inlet and outlet of the capillary can be drastically different. They are also limited to relatively high shear rates. Falling-body and vibrating devices can be very accurate but are limited to low-viscosity Newtonian liquids [27]. The rotational devices are the most common because they are able to give well-defined shear rates. For such rheometers, the means of inducing the flow are two-fold: One can either drive one member and measure the resulting couple or else apply a couple and measure the subsequent rotation rate. the former was introduced by Couette in 1888 and the latter by Searle in 1912. There are two ways that rotation can be applied and the couple measured. The first is to drive one member and measure the couple on the

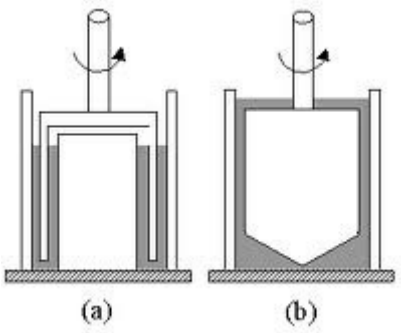

FIGURE 2.11: Concentric cylinder (a) double gap (b) Mooney

same member [1], whilst the other method is to drive one member and measure the couple on the other [3]. Unfortunately, high pressure rotational devices are difficult to design because viscoelastic or rotational information must be transferred under pressure. Mechanical information is often lost via transfer of torque through a dynamic seal, limiting measurement sensitivity. Additionally, a magnetically coupled drive shaft, which generates slightly non-uniform flow, is often used for motion control. The sample can often leak out of the measurement device and penetrate the head space due to sample swelling, or high shear rates, creating measurement errors [28]. In figure 2.11 two types of Couette or concentric systems which are used in this experiment are shown. The first one is the double gap and the second the Mooney system. If the gap between these two concentric cylinders is small enough and the cylinders are in relative rotation, the test liquid enclosed in the gap experiences almost constant shear rate. Furthermore if the the radii of the outer and inner cylinder are r_0 and r_i, respectively and the length of the bob is L, the local change in the tangential velocity across a small liquid element dr at r from center line of the bob is the local shear rate $= rd\omega$/dr and the shear stress in the element is $\sigma = \eta r d\omega$/dr for Newtonian fluid. The moment of the drag force is the sum of the stress in each element multiplied by the area of

[1] Like Aton paar rheometer MCR 300 which used in this experiment.

the cylindrical surface times the distance r

$$M_{cc} = \text{sum of } (2\pi L r^2 \text{ stress from each element}) \tag{2.23}$$

To calculate the angular velocity of the outer cylinder, all contributions from the static cylinder to the moving one are summarized:

$$\int_0^{\Omega} d\omega = \frac{M_{cc}}{2\pi L \eta} \int_{R_i}^{R_0} \frac{dr}{r^3} \tag{2.24}$$

so that

$$\Omega = \frac{M_{cc}}{4\pi L \eta} \left[\frac{1}{R_i^2} - \frac{1}{R_0^2} \right] \tag{2.25}$$

and in terms of viscosity:

$$\eta = \frac{M_{cc}}{4\pi L \Omega} \left[\frac{1}{R_i^2} - \frac{1}{R_0^2} \right] \tag{2.26}$$

From equation 2.23, the stress at r is

$$\sigma = \frac{M_{cc}}{2\pi r^2 L} \tag{2.27}$$

and so the shear rate for a Newtonian liquid is

$$\dot{\gamma} = \frac{\sigma}{\eta} = \frac{2\Omega}{r^2} \left[\frac{1}{R_i^2} - \frac{1}{R_0^2} \right]^{-1} \tag{2.28}$$

If the gap is small, we can make the approximation $(R_0 + R_i) \approx 2R_0 \approx 2R_i$ and then the shear rate is

$$\dot{\gamma} \approx \frac{\Omega R_0}{(R_0 - R_i)} \tag{2.29}$$

and from 2.27 and 2.29, we see that the viscosity is given by

$$\eta = \frac{C(R_0 - R_i)}{2\pi R_0^3 \Omega L} \tag{2.30}$$

To have same the shear rate at the bottom of the cylinder, a cone can be selected as the shape of the end of the cylinder. In operation, the tip of the cone should just touch the bottom of the outer cylinder container. The cone angle($\alpha = \arctan[\frac{(R_0 - R_i)}{R_0}]$) is such that the shear rate in the liquid trapped between the cone and the bottom is the same as that in the liquid between cylinders. This arrangement is called the Mooney system and it is relatively easy to use and clean [3, 22].

2.3.4 Taylor Number and Reynolds Number

Taylor number is a dimensionless group associated with viscous instabilities in circular Couette flow, the value of which depends on the the kinematic viscosity and on the radii and velocities of the cylinders [3]. When the liquid is in a small gap and laminar flow, any small element of the liquid is in constant velocity known as streamlines. The translational velocity of the element is the same as that of the streamline at its center. There is of course a velocity difference across the element equal to the shear rate and this shearing action means that there is a rotational or vorticity component to the field. When the shear rate reaches a critical value, secondary flows occur, which consist of ring-like vortices associated with instability in circular Couette flow. This of course enhances energy dissipation and can be seen as an increase in the stress over what we expect. The Taylor number can be shown by

$$Ta = \Omega_c \left(\frac{R_0 + R_i}{2} \right)^{1/2} \frac{\rho (R_0 - R_i)^{3/2}}{2\eta} \tag{2.31}$$

Taylor vortices are stable secondary flows, unlike turbulent flows in which the velocity components show random variation. At high shear rates the secondary flows become chaotic and turbulent flow occurs. This happens when the inertial

forces exceed the viscous forces in the liquid. This is expressed by Reynold's number which is the ratio of inertial forces to viscous forces. For the Couette system Reynold's number is given by

$$Re = \frac{\Omega_c(R_0 + R_i)(R_0 - R_i)\rho}{2\eta} \tag{2.32}$$

and in terms of shear rate

$$Re \approx \dot{\gamma}\frac{(R_0 - R_i)^2\rho}{\eta} \tag{2.33}$$

It is important that we know at what Reynold's number our instrumental configurations give turbulent flow and work below this, otherwise we will think that shear thickening is occurring [3, 22]

2.4 Particulate suspension

A suspension or dispersion is a fluid containing particles in a liquid medium. When the size of the particles are small, this is called colloid, When suspended particles are non-spherical, they can be oriented by a flow field and they produce much stronger elastic effects than with a suspension of spherical particles at a similar volume fraction [29].

Chapter 3

Experiment

3.1 Experimental set up

This high pressure rheology experiment was carried out at Laboratory for Soft and Complex Matter at NTNU. A rheomter was the main instrument for measuring using a high pressure cell including double gap and Mooney geometry. The pressure cell was connected to a syringe pump which was used to pressurize the carbon dioxide into the cell. The source of carbon dioxide was ultra pure CO_2 from Yara Idustrial AS. The schematic of the set up is shown in figure 3.1.

3.1.1 Rheometer

The rheometer was an MCR 300 manufactured by Anton Paar. This rheometer relies upon an air bearing for its precision. In this study, the rheometer measured shear viscosities, shear rates and shear stresses by imposing shear stress through controlled torque and measuring angular motion or imposing shear rate through controlled speed and measuring torque. The manufacturer's software US200 was used to calculate shear stresses and shear rates. According to manufacturer specifications, the rheometer has a frequency range from 10^{-4} to 100 Hz, a speed

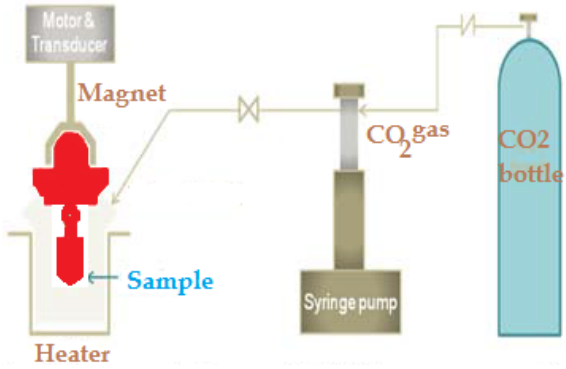

FIGURE 3.1: Experimental set up including high pressure cell, syringe pump and CO_2 bottle

range from 10^{-5} to 1200 1/min, and a torque range from 0.02 μNm to 150 mNm, with a resolution of < 0.001 μNm. The rheometer is compatible with several geometry accessories; this study involved a high pressure cell with double gap Couette (Concentric Cylinder) and Coaxial cylinder measuring systems(Mooney) [30, 31]. In figure 3.2 the rheometer and the pressure cell are shown.

3.1.2 High-Pressure Attachment

The rheometer used in this work has a high pressure attachment developed by Paar Physica. The high pressure cell allows measurements at pressures up to 400 bar and up to 200°C. In the pressure cell, the measurement area is completely sealed against the environment. Therefore, a magnetic coupling is used to transfer the torque from the instrument motor to the measuring system. The outer magnet is mounted onto the rheometer drive in place of the usual measuring system (see figure 3.2) where magnetic coupling conveys the torque of the measuring drive to the pressure head. The measuring system inside the cell is attached to a low-friction mechanical bearing. The system allows measurements at a minimum torque of

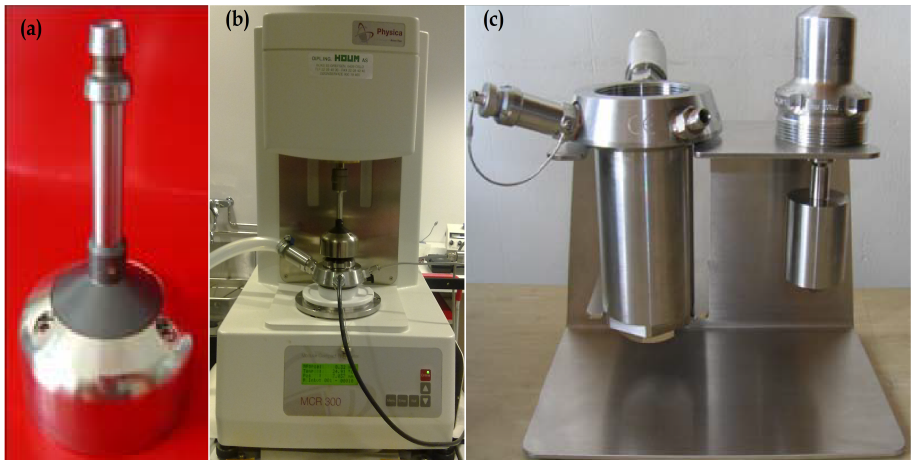

FIGURE 3.2: The rheometer uses magnetic coupling to transfer torque from instrument motor to the pressure cell. (a) Magnetic coupling (b) The high pressure cell mounted in the Physica MCR 300 (c) Pressure cup and Head with Mooney geometry

100 μNm[1], and the coupling can transmit torques up to 150mN.m[2]. The maximum speed is 1200 rpm. The bearings are high-precision miniature ball bearings. They are used dry, and to minimize the friction, the normal force is maintained at $\pm$ 0.1N. The pressure cell is preferably used for rotational measurements such as flow curves or time tests. Oscillatory measurements are possible only in a limited range and at high-amplitude or large deformations. Therefore, they can only be carried out at samples with a broad linear viscoelastic range. Temperature ramps can be carried out at low heating/cooling rates only because of the comparatively large mass of the pressure cell [27, 32].

[1] the rheometer minimum torque is $0.02\mu Nm$

[2] Which was the maximum torque of the Paar Physica MCR 300

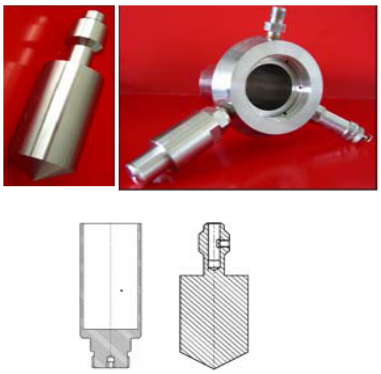

FIGURE 3.3: Coaxial cylinder measuring system CC33.2/PR [34].

Coaxial cylinder measuring system (CC33.2/PR)

Measuring systems including cup and bob come in various forms such as coaxial cylinder, double gap, etc. DIN standard coaxial cylinders(Fig 3.3) are referred to by the diameter of the inner bob. For instance in this experiment CC33.2 refers to a coaxial cup and bob having a 33.2mm diameter bob. The diameter of the cup is 36.00mm which is in proportion to the bob size as defined by the DIN Standard. The gap between the cylinders must be very slightly larger than the gap at the edge of the cone and plate if a constant shear rate is required. Cup and bob measuring geometries require relatively large sample volumes and are more difficult to clean. They usually have a large mass and large inertia and so can produce problems when performing high frequency measurements. Their advantage comes from being able to work with low viscosity materials and mobile suspensions. Their large surface area gives them a greater sensitivity and so they will produce good data at low shear rates and viscosities. The ISO Standard of CC is 3219 [32, 33].

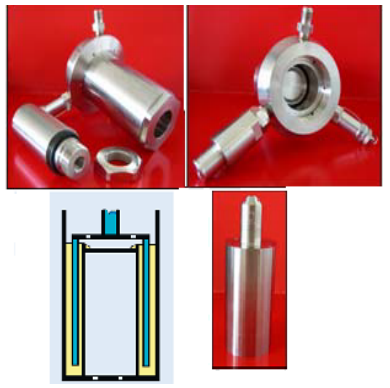

FIGURE 3.4: Double gap concentric cylinder measuring geometry DG35.12/PR [34].

Double gap measuring system (DG35.12/PR)

The double-gap measuring system is a concentric cylinder system designed for tests on low-viscosity liquids. It has the largest surface area and is therefore ideal for low viscosity /low shear rate tests. According to the standard geometry (DIN 54453), an inner cylinder is mounted in the center of the cup. The cross-section of the cup is shown in figure 3.4. The bob has the shape of a hollow cylinder (like a“short pipe”) therefore showing both an inner and an outer surface. Due to this increased shear area, lower torques can be determined compared to a more typical cylinder like the Coaxial cylinder standard ISO 3219. A disadvantage of this geometry is the time-consuming cleaning procedure. It should be noted that the inertia of some double gap systems may severely limit the top working frequency in oscillatory testing [33, 35].

Pressure and temperature sensor

To measure pressure inside of the cell a pressure sensor PA-23/400Bar made by Keller Druckmesstechnik is used. It is connected to the pressure supply unit and

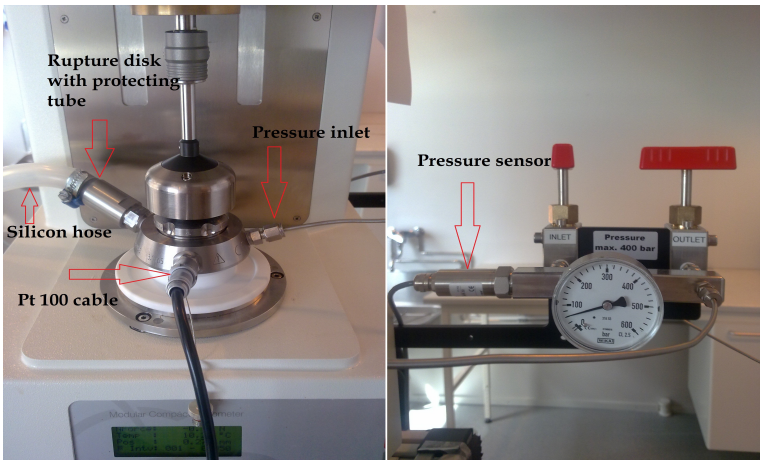

FIGURE 3.5: (a) Pt100 cable for reading the temperature (b) pressure sensor for measuring pressure.

calibrated with a syringe pump via software US200. To read the temperature inside the cell a Pt100 cable is used, this is connected to the pressure cup and is calibrated by rheometer softwar US200. Both pressure sensor and Pt100 are shown in figure 3.5.

Pressure head

The pressure head in the high pressure cell has a crucial role in establishing the accuracy of the measurement, because of the two miniature ball bearings located inside the head which transfers torque from the rheometer to the inside of the cell by magnetic coupling. Normally before each experiment their friction is checked and if there were bad bearings, they were cleaned or changed with new ones. In figure 3.6 the pressure head and the two ball bearing inside the pressure head are shown.

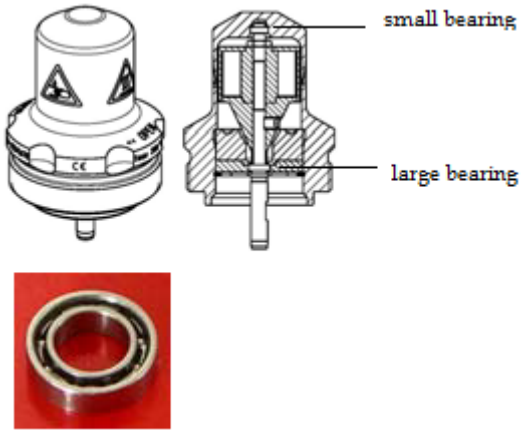

FIGURE 3.6: Pressure head and ball bearing located inside of the head [34].

Syringe Pump

The TELEDYNE ISCO 260D syringe pump is designed specifically for refilling under high pressure and pressure programming to handle liquid and supercrtical CO_2 and other fluids (figure 3.7). It consists of a controller and pump module with pressure range from 0.7 to 517.1 bar with an accuracy of $\pm 0.5\%$ (of full scale at constant temperature) and a flow rate range from 0.001 to 107 ml/min with an accuracy 0.5% of setpoint. The 260D syringe pump controller offers many different operating modes. The standard operating modes are: Constant flow, Constant pressure, flow or pressure programming and external control [36].

High shear rates on low viscosity materials

The angular position / speed sensing system in controlled stress rheometers will have a maximum 'tracking' rate before it is no longer able to measure the angular velocity correctly. If this velocity is exceeded the instrument will normally indicate some sort of over speed error. If this happens at shear rates lower than we

FIGURE 3.7: TELEDYNE ISCO Syringe Pump 260D

would like to obtain, the measuring geometry should be changed to a one with a smaller gap (a decrease in gap will increase the shear rate for the same angular velocity.) The highest shear rates can be obtained with a parallel plate with a very small gap or a tapered plug system. For low viscosity materials and mobile suspensions a cup and bob type system should be used. Maximum sensitivity is obtained with a double concentric cylinder (double gap).

3.2 Experimental method

Carbon dioxide in gaseous state was introduced to the high-pressure cell through an inlet port near the top of the cell (see figure 3.5) - the pressure inlet connected to the syringe pump. The source of carbon dioxide was a pure CO_2 from Yara AS. The pump maintained a fixed pressure, and the pressure transducer was used for reading the pressure. The temperature was controlled through the wall and read

through the head of the cell with the temperature sensor PT100. The rheometer rotation is guided by an air bearing, but the high pressure cell requires high-precision ball bearings which limit accurate measurements to signals above 100μNm. The mechanical ball bearing was checked at the beginning of every measurement and it had to be between $\pm 50\mu$Nm. The minimum pressure and temperature inside of the cell was 60 bar and 10°C. According to the phase diagram for carbon dioxide (2.6) at this pressure and temperature the cell contains liquid carbon dioxide. The cell is designed to function with liquids and the existence of a gas in the cell would damage the ball bearings. 60 bar pressure and 10°C was the minimum required for the mixing of clays and carbon dioxide.

Sample filing and mounting

The clays including Laponite, Quick clay, Kaolinite, Na-Fluorohectorite and Na-Montmorillonite were ground with a mortar and pestle and dried in a vacuum oven for 12 hours at 130°C. To have an exact amount of dry clay, it was weighed before and after drying, and any more than the desired amount was removed. The pressure cup was filled with clay samples after the filling adapter had been inserted to the cup to avoid spilling samples on the O-ring or thread of the pressure cup. After sample filling the filling adapter was removed and the O-ring checked for mechanical damage and signs of wear. If the O-ring was undamaged, it could then be placed in the groove of the pressure cup. Then the pressure head with the Mooney or double gap mounted measuring system was placed onto the thread of the pressure cup and fastened very tightly and was returned to the oven at 130°C for a period to remove any humidity absorbed during the filling. The pressure cell should not be tilted after filling because the clay powder could get into the pressure head and damage the rotation parts and ball bearings. However the completed pressure cell was inserted into the measuring cell in the way shown in figure 3.5. The rupture disc and silicon hose were connected to the cell for safety reasons in the event of over pressurization. Then after connecting the cell to the pump, immediately a vacuum pulled on the sample to remove any air from the system

and this was followed by pressurization with carbon dioxide. The temperature was kept at 10°C while pressurization was carried out.

Rheological measurements

To make rheological measurement of liquid carbon dioxide and clays, the clays are dissolved into the liquid carbon dioxide by stirring for 15min with the measurement system under 500rpm. Bubble formation should be avoided, so we used a moderate speed compared to the highest speed of 1200rpm. After that any shear treatment or occasional stirring was eliminated by subjecting each sample to a pre-shear of 50 1/s for 2min, followed by a 2min rest period. Many measurements were done at 60bar and 10°C. In some cases measurements were carried out at different pressures and temperatures, but we had to be careful to work in the liquid phase and should avoid the area close to the liquid-gas line in the phase diagram. It is important to have liquid inside of the cell because the rheometer is designed to work with liquid not gas.

Chapter 4

Data analysis and results

4.1 Checking of the friction of the ball bearing

The first measurement was to check the friction of the ball bearing. The mechanical bearing in the pressure head contributes significantly to the torque measured by the instrument during a measurement. To keep this contribution as small as possible, the bearings have to be in good condition and a motor adjustment has to be carried out first. The friction check should be carried out regularly. This has to be done before every experiment. The torque hysteresis of good mechanical bearings should be smaller than $\pm 50 \mu \mathrm{Nm}$ [32]. The figure 4.1 shows data from a good bearing. If the measured torque is out of the range, the ball bearings should be cleaned and the motor adjustment should be repeated. If this is not successful, the ball bearings must be replaced with new ones.

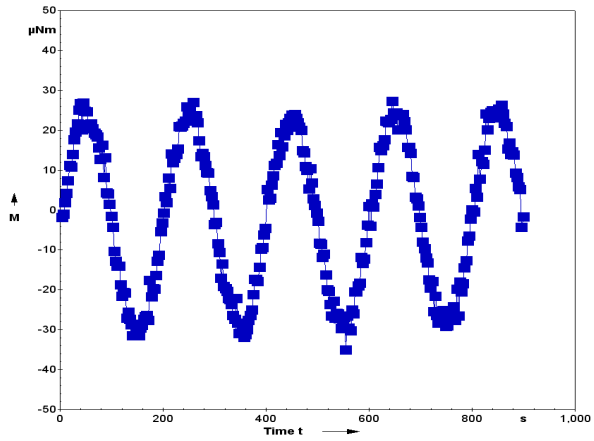

FIGURE 4.1: Good ball bearing check

4.2 Rheology of clay and CO_2 in the double gap system DG35.12/PR

Distiled water, silicon oil and pure carbon dioxide

After checking the ball bearings, to ascertain the accuracy of the double gap system, the viscosity of the distiled water and silicon oil were measured. In figure 4.2 the viscosity of the distiled water versus time in constant shear stress is illustrated. The plot shows that double gap geometry can measure water viscosity with high accuracy. However it can be seen that the shear thinning at the beginning is due to magnetic coupling. The silicon oil used was Dow Corning 200/10cS which has a viscosity of 10mPas. The same measurement, as was done with distiled water, was made, but this time with applied shear rate. We applied shear stress to measure the viscosity of water because in the CSS (Control shear stress) mode, the inertia of the system can be compensated for. This can be done by using software US200 connected to the rheometer. In most cases when the viscosity was so low we compensated for inertia in CSS mode to avoid the effect of inertia. Figure 4.3

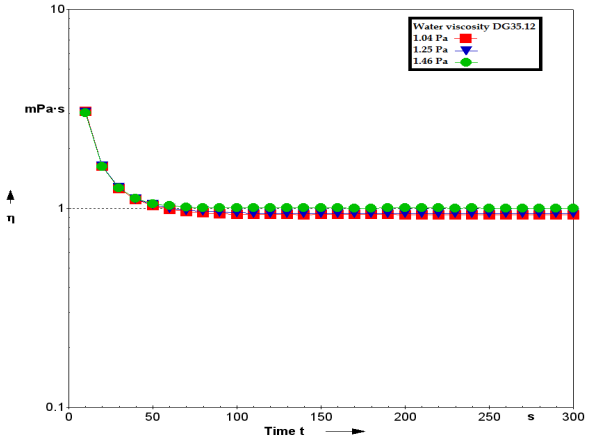

FIGURE 4.2: The viscosity as a function of time for the double gap high pressure cell containing distilled water at ambient atmosphere., sheared at constant shear stress 1.04, 1.25 and 1.46 Pa. The correct viscosity for distilled water is about 1 mPas.

illustrates the viscosity of silicon oil vs time.

Van der Gulik [37] measured the viscosity of carbon dioxide using a vibrating viscometer [1]. The viscosity of carbon dioxide in 7 °C and 60 bar is approximately 0.1 mPas. We liquefied carbon dioxide at 60 bar pressure and 10 °C, so we should have had a viscosity of 0.1 mPas in this condition. Our Double gap cell has the limitation of measuring viscosity to 0.2 mPas. It is not possible to measure the viscosity of carbon dioxide in this condition, but in the author's experience, this is at the limit of the measurement range, so it is difficult to trust it. Nevertheless, we inserted carbon dioxide gas and pressurized it to the desired condition and tried to measure viscosity as a function of time and shear rate which is shown in figure 4.4. This seems to show a shear thinning, but we should consider that carbon dioxide viscosity in this condition is under the limit of our instrument and

[1] Van der Gulik used vibrating-wire viscometer which set a thin tungsten wire into transversal vibration and determined the damping of this motion by the surrounding sample liquid [37].

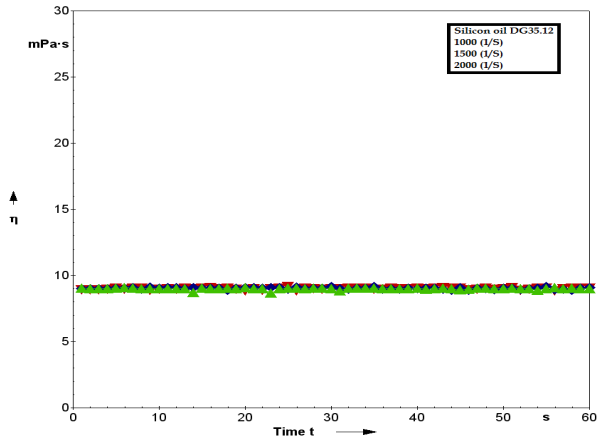

FIGURE 4.3: The viscosity as a function of time for the double gap high pressure cell containing Silicon oil Dow Corning 200/10cS at ambient atmosphere, sheared at constant shear rate 1000, 1500 and 2000 1/s. The correct viscosity of silicon oil 200/10cS is 10mPas.

the result is not trustable.

The Clays and liquid carbon dioxide dispersion in the DG35.12/PR

The optimum amount of clay that we could add to the double gap cell was 0.3gram. For more or less than this amount it was difficult to measure the dispersion viscosity. However this problem was solved with the Mooney measurement system CC33.2/PR allowing us to use different amounts of clay. Because of this limitation in the double gap measurement system, different types of clay were used such as Laponite, Quick Clay, Na-Fluorohectorite and Na-Montmorillonite. Each experiment was done two times for each clay to be sure the results were reproducible. The viscosity of different types of clay as a function of shear stress is shown in figure 4.5 and the flow curves are shown in 4.6. Then we limited our testing to two types of clay, Laponite and Quick clay, for viscosity variation with

4.2 RHEOLOGY OF CLAY AND CO_2 IN THE DOUBLE GAP SYSTEM DG35.12/PR

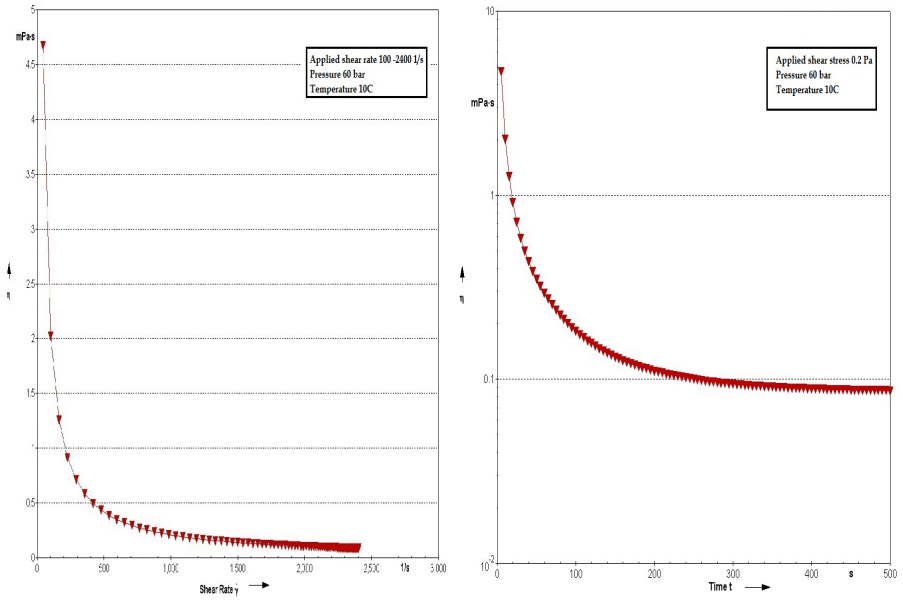

FIGURE 4.4: liquid carbon dioxide in 60bar and 10c (a) viscosity versus shear rate 100 to 2400 1/s (b) viscosity versus time. Applied Shear stress 0.2 Pa

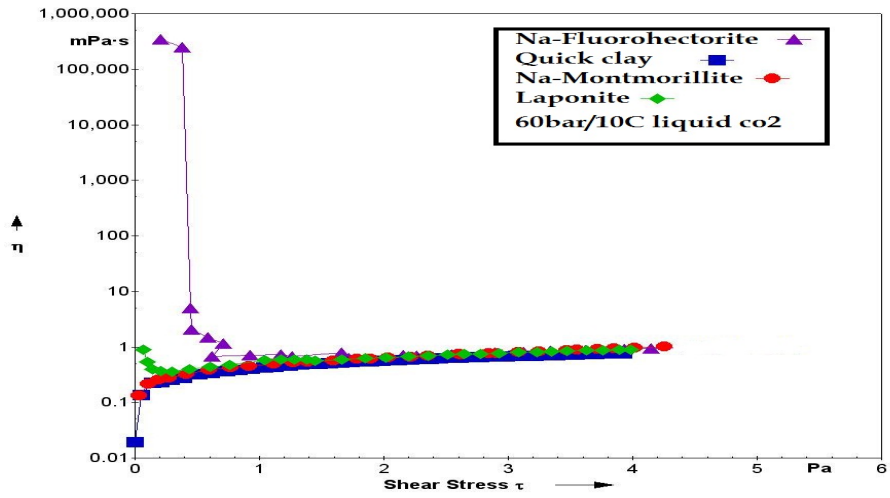

FIGURE 4.5: Viscosity as a function shear stress for different type of clay, Na-Fluorhectorite, Quick clay, Na-Montmorillite and Laponite in pressure 60 bar and temperature 10 °C.

time. These are shown in the figure 4.7 and 4.8. The last measurement with the double gap measurement system was of laponite dispersed in liquid CO_2 in different pressures. Viscosity as a function of shear stress is illustrated in figure 4.9. When we added different types of clay to the double gap, from 4.5 it is clear that the clay normally can increase the viscosity, irrespective of type of clay and for Na-flouhectorite there is yield stress but probably this is due to magnetic coupling or swelling of clay to the ball bearings. For Laponite and Quick clay in constant shear rates, viscosity versus time is almost Newtonian, but there is a shear thickening in high shear stress which due to the effect of turbulence. We tried to avoid shear rates which cause turbulence or secondary flow inside the cell by using the lowest possible shear rates.

4.2 RHEOLOGY OF CLAY AND CO_2 IN THE DOUBLE GAP SYSTEM DG35.12/PR

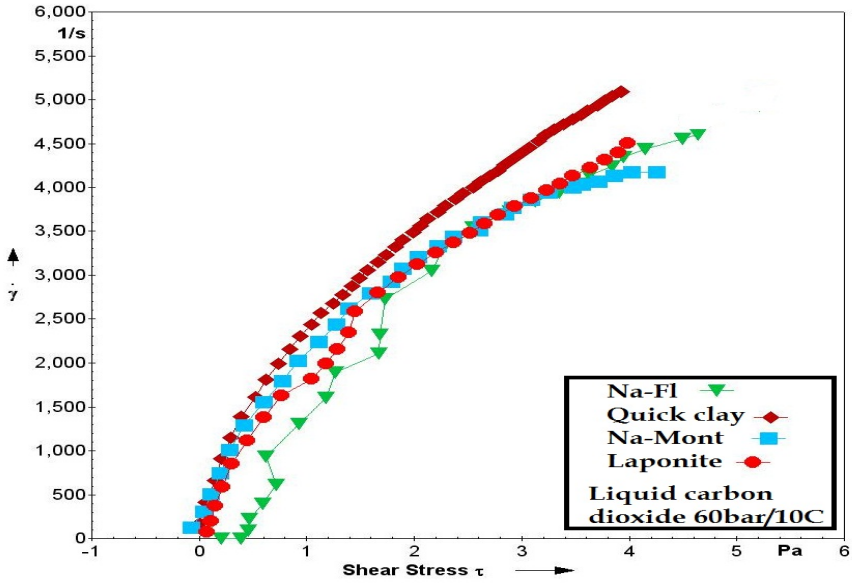

FIGURE 4.6: Flow curve for four different type of clays, including Na-Fluorhectorite, Quick clay, Na-Montmorillite and Laponite. Pressure 60 bar and temperature 10 °C.

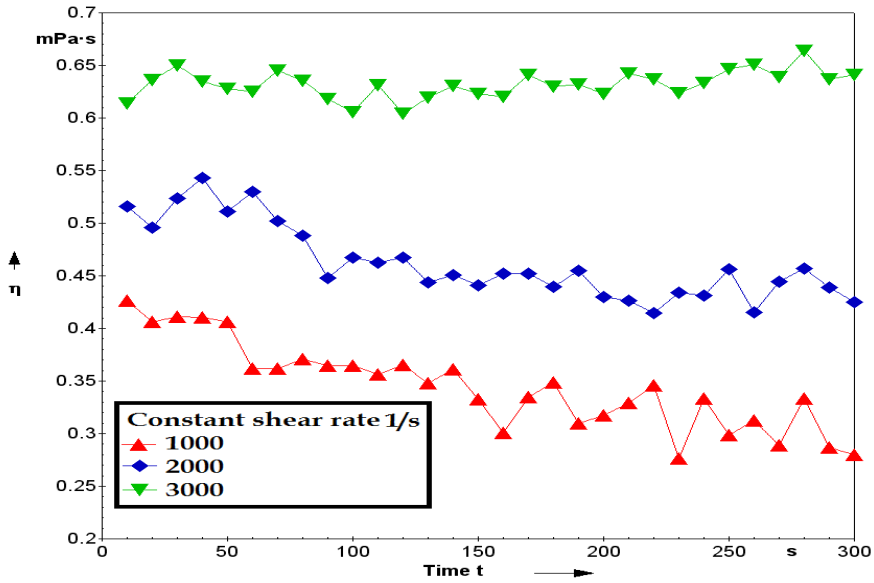

FIGURE 4.7: Viscosity behavior 0.3gram laponite and liquid CO_2. Shear rate applied 1000, 2000, 3000 (1/s). Pressure 60 bar and temperature 10°C.

4.2 RHEOLOGY OF CLAY AND CO_2 IN THE DOUBLE GAP SYSTEM DG35.12/PR

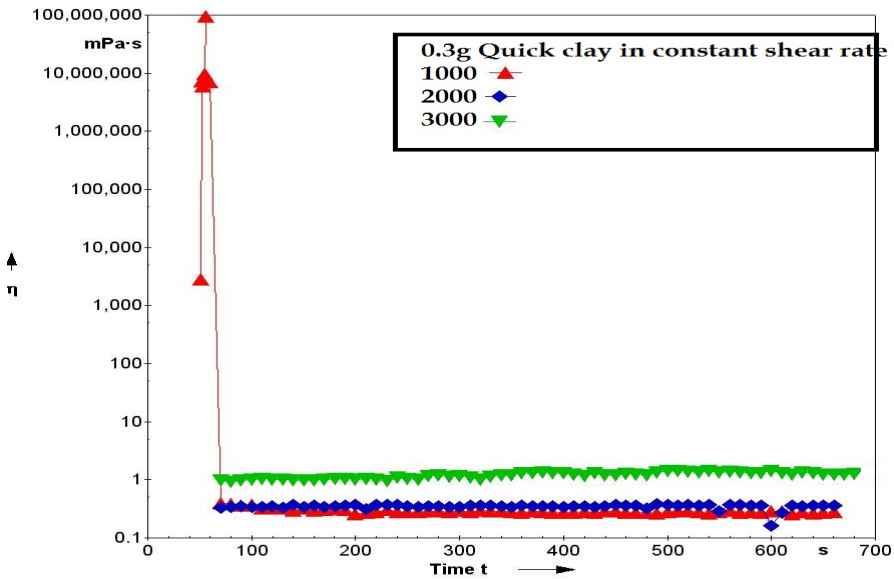

FIGURE 4.8: Viscosity behavior 0.3gram Quick clay in the liquid CO_2 versus time. Shear rate applied 1000, 2000 and 3000 (1/s). Pressure 60 bar and temperature 10 °C.

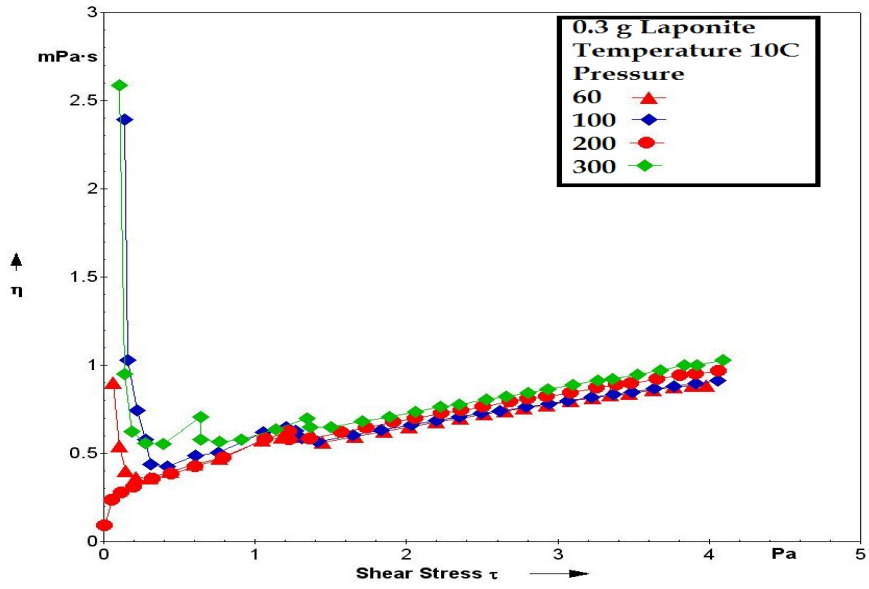

FIGURE 4.9: Variation of viscosity with shear stress with different pressure from 60bar to 300bar, temperature 10°C

4.3 Rheology of clay and CO_2 in the coaxial cylinder system CC33.2/PR

Distiled water and silicon oil

The coaxial cylinder system or Mooney system was used for this experiment because it had a larger sample volume $\approx$ 30ml compared to $\approx$ 5.81ml in the double gap system. The coaxial system does not have the limitations of the double gap system, but we have to inject more carbon dioxide gas to the cell to reach the desired pressure and temperature which was 60 bar and 10°C. Before each experiment the friction of ball bearings was checked. Then the viscosity of distiled water and silicon oil measured with the Mooney cells and the results are given in figure 4.10. This figure shows the viscosity of distiled water as a function of time at different applied shear stresses. The viscosity of distiled water should be 1 mPas but our measurement is higher than this. So in the low viscosity range we have this measurement error. The viscosity for silicon oil 200/10cS is shown in figure 4.11. The viscosity of silicon oil should be 10mPas. The measurement error is less than water, which was 3 times greater than 1 mPas but for silicon oil is $\approx$ 10% greater than 10mPas.

The Clays and liquid carbon dioxide dispersion in CC33.2/PR

We had to find the best amount of clay that could work with this geometry. We focused on two types of clay: Quick clay and Laponite. 3gram and 5gram of Quick clay were tested. The capacity of the cell was 30.4ml liquid, and we had to inject carbon dioxide to reach the 60 bar at 10°C. We increased pressure to see how the viscosity was effected. The figures 4.12 and 4.13 shows the flow curve and viscosity as functions of shear stress. We tried to add 10gram of Quick clay to the cell and dissolve it with liquid carbon dioxide, but during stirring the ball bearing inside of the pressure head was damaged and we concluded that 10 gram of Quick clay was more than cell capacity. Viscosity measurement of laponite

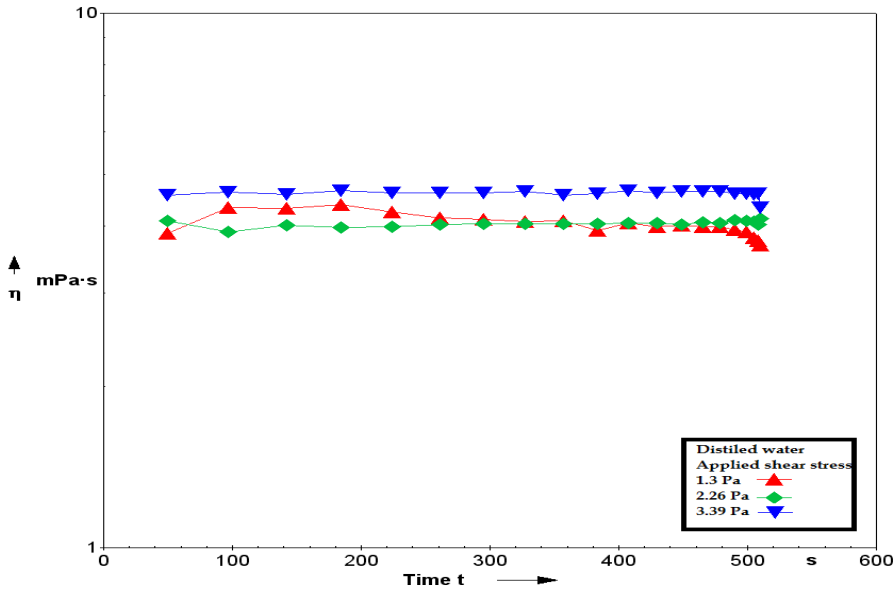

FIGURE 4.10: The viscosity as a function of time for the Mooney high pressure cell containing distilled water at ambient atmosphere, sheared at constant shear stress 1.3, 2.26 and 3.39 Pa. The correct viscosity for distilled water is about 1 mPas.

4.3 RHEOLOGY OF CLAY AND CO_2 IN THE COAXIAL CYLINDER SYSTEM CC33.2/PR

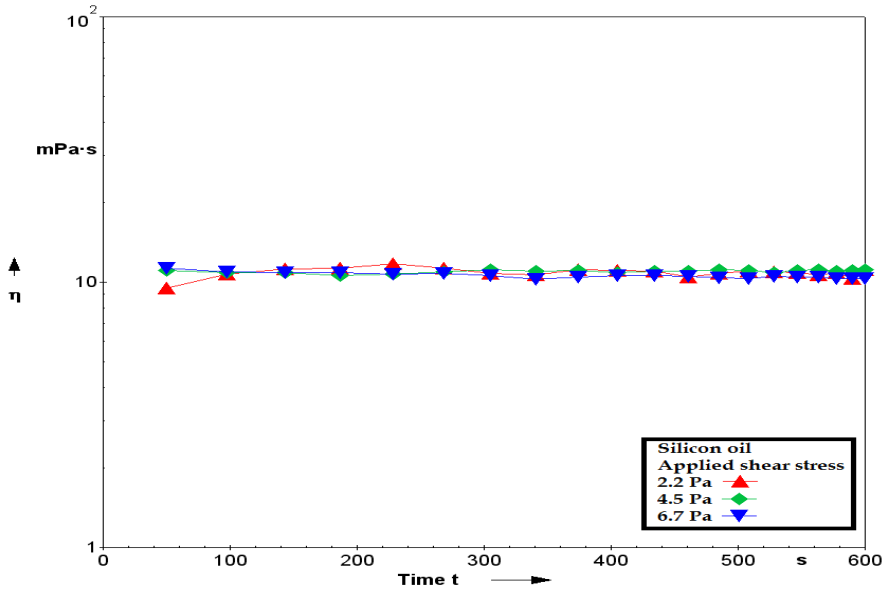

FIGURE 4.11: The viscosity as a function of time for the Mooney high pressure cell containing distilled Silicon oil Dow corning 200/10cS at ambient atmosphere, sheared at constant shear stress 2.2, 4.5 and 6.7 Pa. The correct viscosity of silicon oil 200/10cS is 10 mPas.

clay and liquid carbon dioxide dispersion were also done. 5 gram and 10 gram of Laponite was poured to the cell and we measured viscosity as a function of shear rate and time. The measurement was carried out at different pressures. For 5gram Laponite both viscosity as a function of shear rate and flow curve is illustrated in figure 4.14. For 10gram Laponite viscosity as a function of shear rate is shown in figure 4.15. These amounts of clay were in the cell when carbon dioxide was injected to the cell. The Mooney cell was used for stirring, although it is not designed for this purpose. We sought to disperse these clay particles into the liquid CO_2, but the viscosity range for different types and amounts of clay is the same, and the reason for this could be that the clays were sedimented in the bottom of the cell and just some of the clay particles became suspended in the liquid to increase its viscosity. However these types of test were repeated several times, and some times we had very high viscosity which shows clays became suspended to a greater extent in the liquid. Intrinsically a high pressure experiment is difficult to handle in comparison to other types of rheology experiment.

4.4 Discussion

A number of groups have reported the effect of high pressure CO_2 on the viscosity of polymers using a rotational rheometer or other types of rheometer [27, 31, 38, 39]. In many articles the high pressure cell was used to measure the viscosity of a colloidal suspension while positive pressure was applied. In these experiments the high pressure cell was usually filled with a *liquidy* sample with significant viscosity, for instance Fumed Silica aerosil 10 Pas, and the shear viscosity or shear modulus was measured under elevated pressure [40]. No articles were found in which a gas was liquefied and stirred with solid particles by a rotational rheometer. However we adopted this method because our aim was to see how clay particles can be incorporated into liquid carbon dioxide. Normally carbon dioxide is a gas in ambient conditions and it has to be pressurized to become liquid. A high pressure cell was necessary for this process. We were unable to

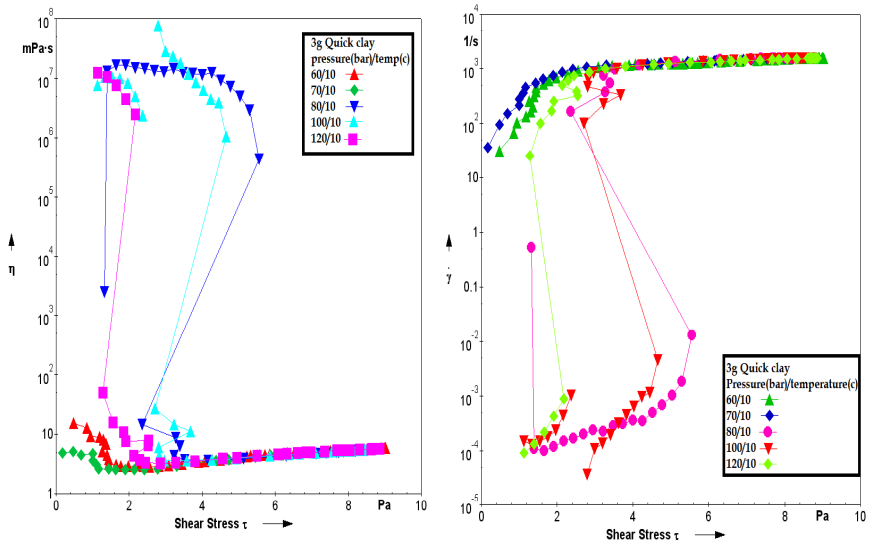

FIGURE 4.12: Viscosity of 3gram Quick clay and flow curve in different pressure. (a) viscosity vs shear stress (b) shear rate vs shear stress. Pressure 60, 70, 80, 100 and 120 bar and temperature 10 °C.

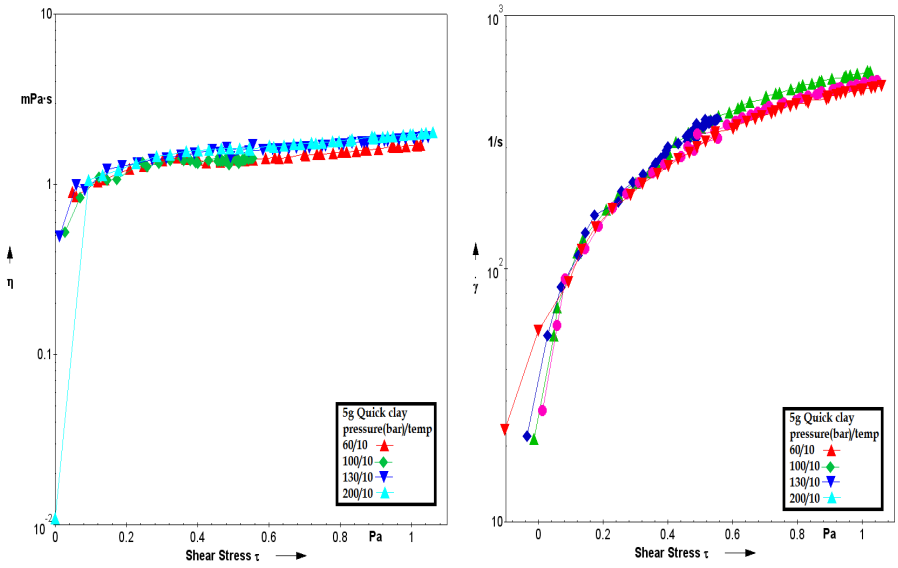

FIGURE 4.13: (a) Viscosity of 5gram Quick clay and flow curve in different pressure (a) Viscosity versus shear stress (b) Shear rate versus shear stress. Pressure 60, 100, 130 and 200 bar and temperature 10°C.

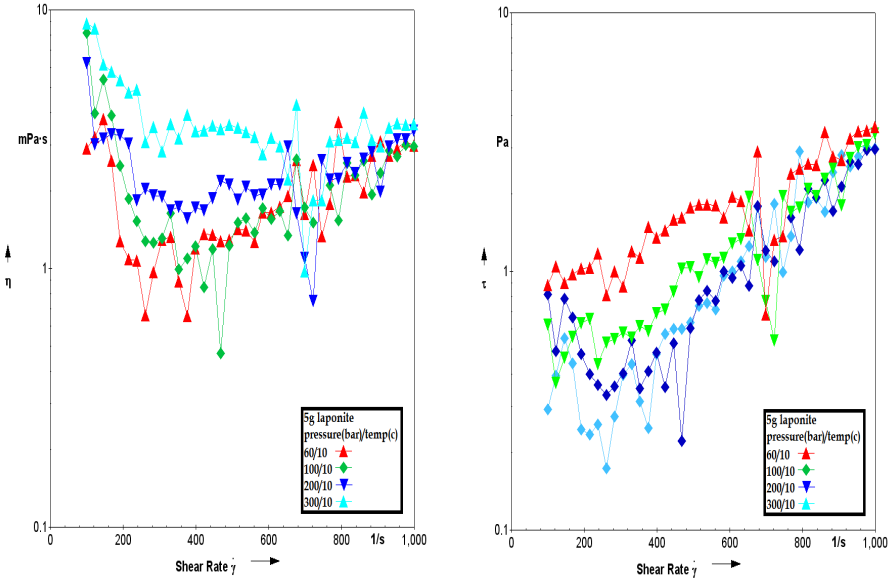

FIGURE 4.14: Viscosity of 5g laponite and liquid carbon dioxide. (a) viscosity vs shear rate (b) flow curve. Pressure 60, 100, 200 and 300 bar and temperature 10°C.

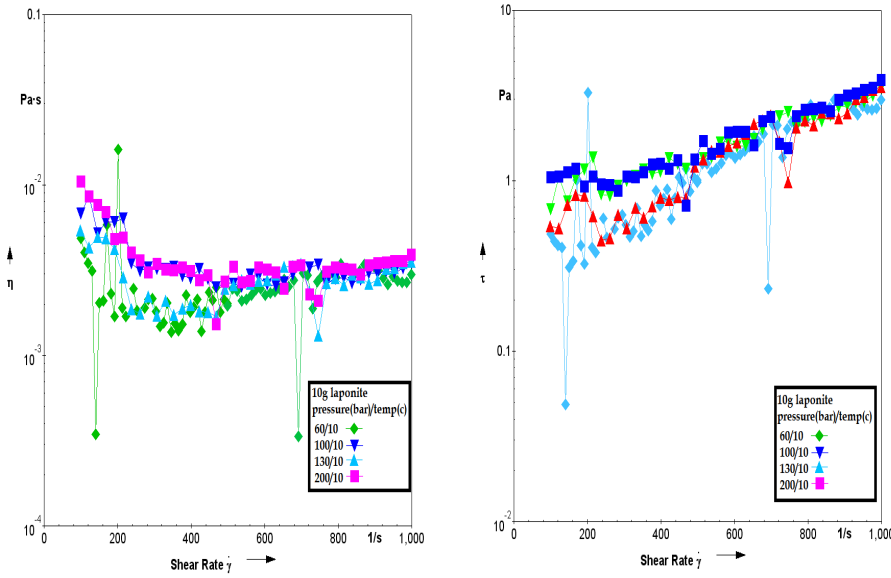

FIGURE 4.15: Viscosity of 10g laponite and carbon dioxide. (a) viscosity vs shear rate (b) shear stress vs shear rate. bar. Applied shear rate 100 to 1000(1/s). Pressure 60, 100, 130 and 200 and temperature 10 °C.

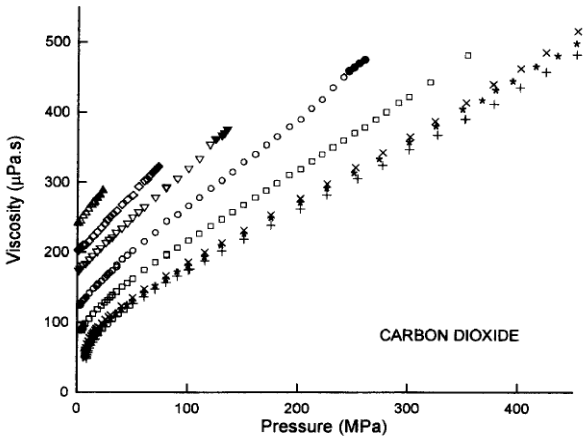

FIGURE 4.16: The viscosity coefficient of carbon dioxide as a function of pressure, open symbols: in the stable state, filled symbol: in the metastable state. △ 220K, Diamond 230K, ▽ 240K, ○ 260K, Box 280K, × 300K, ⋆ 303K, + 308K. From [37].

measure liquid carbon dioxide viscosity because of the limitation of our measuring instrument, although we know of the viscosity of carbon dioxide [2] as a function of pressure from [37]. This is shown in figure 4.16. Thus it can be seen that the viscosity is between 0.1 mPas<η<0.2 mPas for pressure range 4 MPa to 100 MPa and temperature 280K. Our experiment was carried out in a pressure range from 6 MPa to 30 MPa at the temperature 10°C. The viscosity of liquid carbon dioxide as a function of pressure from 40 bar to 320 bar in 280K is shown separately in figure 4.17. Indeed this is the viscosity of the continuum phase in our experiment. The continuum phase has a maximum viscosity of 0.14mPas. When the clays were dispersed in the liquid CO_2, a higher viscosity was measured. As a result we can say that this increase is due to clay particles suspended in the medium fluid. Usually an addition of colloidal particles leads to an increase in viscosity above that

[2] http://www.carbon-dioxide-properties.com/CO2TablesWeb.aspx is a website at which the properties of carbon dioxide are given.

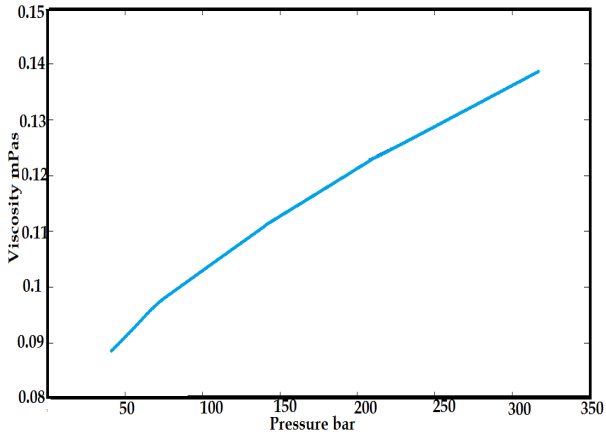

FIGURE 4.17: Viscosity of carbon dioxide in pressure range 40 to 320 bar, temperature 280 K. Data from [37].

of a pure liquid. If we assume there is a homogeneous dispersion inside the cell and the clay particles are non-interacting in liquid carbon dioxide, we should have a moderate increase in the viscosity. In fact we found this increase in the viscosity in this experiment. The results also show the viscosity is shear dependent which has been defined as non-Newtonian behavior. Some instrumental issues should be elucidated firstly which might explain the shear thinning or thickening in our results. Firstly some information might be lost by using magnetic coupling, and this could be the reason for the shear thinning at low shear area in most of the figures. Secondly the clay-CO_2 suspension can enter the pressure head and affect the ball bearing and change the accuracy of the measurement. This problem is always present in the high pressure rotational rheometer and there is no way to avoid it. In figure 4.4 one can see a shear thinning at low shear rate or stress which becomes Newtonian at high shear rate. The shear thinning might be due to magnetic coupling, because liquid carbon dioxide is a Newtonian fluid and its viscosity should not change with shear rate or stress. Actually at high shear rate

or stress a Newtonian region can be seen where the viscosity is 0.1 mPas.
To explain the results in the double gap system, sample filling, which was not easy, should be described first. Different methods were tested to fill the cell with certain amounts of clay. If more than 0.3 grams of clay was added the magnetic coupling was not able to transfer the torque from the instrument into the cell, and for less than 0.3 grams the viscosity was under the limit of our measuring instrument. The best method to fill the cell was to divide the clays between two gaps inside the cell. However, this method was time consuming and thereafter the sealed cell had to be returned to the oven for a period to remove any humidity. From figure 4.5 it can be seen that there is shear thickening at the high shear stress area which could be due to a turbulence effect or the inertia of the system, although the inertia was compensated for by the CSS mode. However it is clear that the viscosity of each clay is higher than the carbon dioxide viscosity (See 4.4) as measured with this system. We should consider the clay stirred in the cell while liquid carbon dioxide existed there. Perhaps we were not able to make a homogeneous suspension because the geometries which were used in this experiment were designed for measuring not stirring. It might be that a part of the clays inside of the cell are incorporated in the increased viscosity and the remainder forms a sediment at the bottom of the cell. One can see from figures 4.7 and 4.8 that the viscosity of laponite and Quick clay-CO_2 are nearly constant with time, and for high shear rates there is higher viscosity which could be due to inertia or a turbulence effect inside the cell. It might be that clay particles react to the flow field and make structures, but in any case the viscosity is increased with high shear rate. The viscosity of 0.3 gram laponite dispersed in liquid carbon dioxide against shear stress is shown in the 4.9. Here shear thickening can be seen, and with increasing pressure the viscosity is increased. If we plot the viscosity as a function of pressure (see figure 4.18) one can see that viscosity is not pressure dependent, and for higher shear stress there is higher viscosity which could be due to inertia of the system, turbulence or secondary flow which enhances energy dissipation and viscosity.

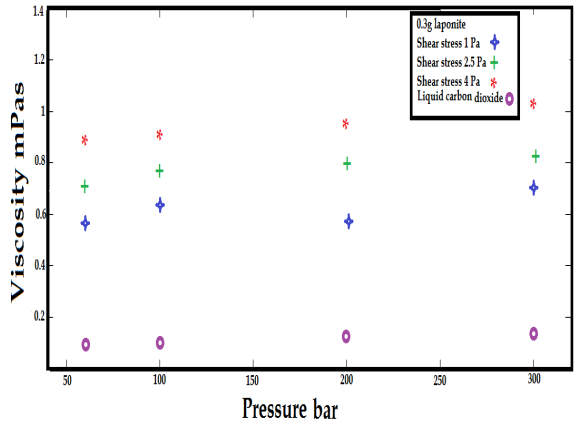

FIGURE 4.18: Viscosity as a function of pressure. 0.3 gram laponite in the Double gap system. Shear stress 1 Pa, 2.5 Pa and 4 Pa.

In the Mooney system, the amount of clay used was more than the double gap system, and because of the incorporation of more clay particles, a higher viscosity was expected. In fact for both types of clay (laponite and Quick clay) which were tested in this measurement system, there are higher viscosity values than for pure carbon dioxide, and they are shear dependent, but the measurement range was within the range that the cell was inaccurate. In this range the viscosity of distiled water is measured 3 mPas instead of 1 mPas, three times more. The viscosity of the clay-liquid CO_2 is within the same range as this system, and we do not have the exact value of the viscosity. We did not have any option but to rectify this inaccuracy and so the data was divided by a factor of three. The original plots were shown in figure 4.12 and 4.13 for Quick clay. The figures shows for both amounts of clay that shear thickening and higher viscosity at higher pressures occur. For 3 grams of clay it seems that the figure shows a yield stress at higher pressures because viscosity is decreasing sharply. This could be due to magnetic coupling or that really there is a yield point at higher pressures. However the viscosity

decreases at low shear and then a shear thickening is observed for 3 grams of Quick clay-CO_2 system (see figure 4.12). There is a moderate shear thickening for 5 grams of clay in the cell,(see figure 4.13). This behavior is different than for 3 grams of Quick clay in the cell. The viscosity versus pressure for 3 grams and 5 grams of Quick clay is shown in figure 4.19. As one can see the viscosity for 3 grams of Quick clay dispersed in the liquid carbon dioxide is higher than 5 grams, and this could be due to the inaccuracy of the measuring system. There is one possibility in which 3 grams of Quick clay particles has more particles incorporated in the dispersion. Therefore one can see the viscosity is increasing with shear. This could be due to the incorporation of the clays, the inertia of the system, or a turbulence effect. The viscosity of Quick clay-liquid CO_2 does not change with pressure, but does change with shear. The sample had low viscosity, so higher shear rates should be applied to measure its viscosity. In fact with these measuring systems the Laminar behavior might be lost in the cell. Consequently secondary flow or turbulence will appear in the cell, and we do not have real viscosity value. This problem can be solved with another type of rheometer.
Two different laponite weights, 5 and 10 grams, were tested with the Mooney system. Figure 4.14 shows that the viscosity versus shear rate for 5 grams of laponite-liquid CO_2 has variation. The only explanation for this is the existence of a non-homogeneous sample inside the cell. However as one can see there is shear thinning at low shear rate for different pressures and shear thickening for high shear rates. The viscosity versus pressure is shown (see figure 4.20) for 5 grams of laponite. The viscosity is higher than pure liquid carbon dioxide and it is pressure dependent. Figure 4.15 shows that the viscosity of 10 grams of laponite in the cell is the same as 5 grams of laponite. The reason for this could be sedimentation of the clay in the cell, and only a certain amount of clay is incorporated in the measurement. Furthermore, the cell was not designed for stirring and perhaps we were not able to stir the sample adequately. But for both amounts of clay there is shear thinning at low shear rate and shear thickening at high shear rate. For 10 gram laponite the viscosity versus pressure is shown in figure 4.20. It seems that

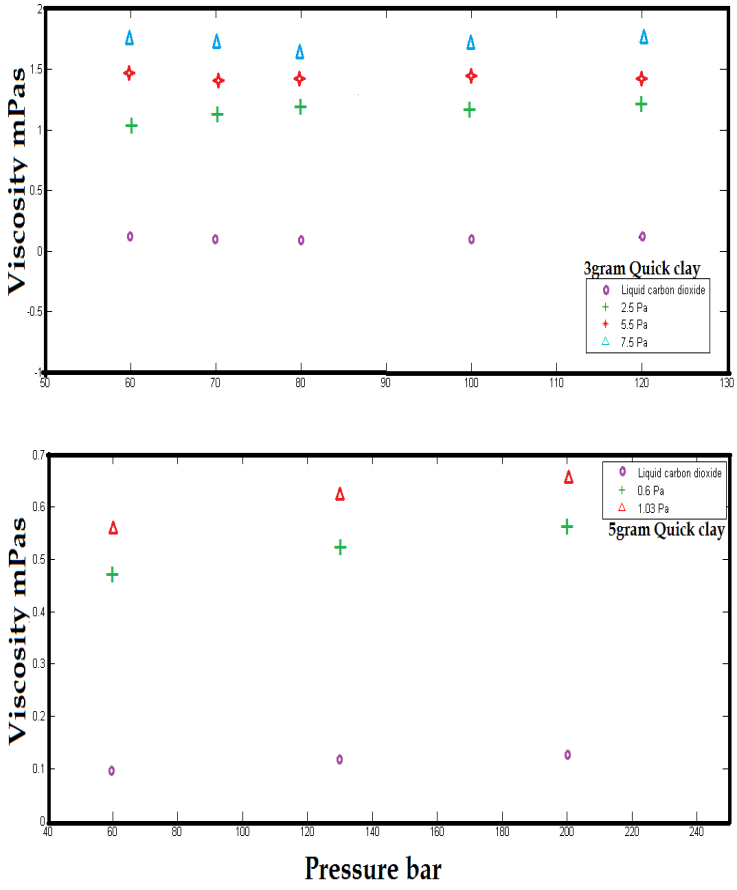

FIGURE 4.19: Viscosity of Quick clay versus pressure in different shear stress. (a) 3gram Quick clay in 2.5, 5.5 and 7.5 Pa shear stress. (b) 5gram Quick clay in 0.6 and 1.03 Pa. Temperature 10°C.

for 10 gram laponite the viscosity is not pressure dependent but seems pressure dependent for 5 gram laponite.

Volume fraction of the sample: A colloidal suspension can be defined using a volume fraction which shows a concentration of particles in the continuum phase. In this experiment it is not possible to make this definition in the same way as for a clay-water suspension. Gaseous CO_2 must be injected into the cell to liquefy the gas. The pressure should be positive to the sample to keep pressure at 60 bar. If we divide, for instance, the weight of the clay by the carbon dioxide weight, we do not find the concentration of the sample inside the cell, but rather the concentration of the clay and carbon dioxide in the cell as well as the pressure head and connected tubes to the pump. In addition, the flow rate to the cell can not be stopped because a pressure of 60 bar is needed in the cell, and if the inlet valve to the cell is closed, the pressure will drop in the cell, and no liquid would be in the cell. In conclusion, the volume fraction can not be defined here and for instance 3 grams of clay in the cell is more accurate definition than 30% concentration in this case.

Ageing test

To see changes over time in the sample, 5 gram laponite was added to the cell under 60 bar pressure and 10°C temperature carbon dioxide. After stirring, the sample was subjected to a shear rate from 10 to 1000 (1/s). The sample was in the cell for six days and was tested three times, on the first, third and sixth days. The pre-shear rate was performed only on the first day. This whole process was carried out three times to be sure of reproducibility. In figure 4.21 the ageing test is shown. One can see the shear thinning at low shear rates and there is Newtonian area at high shear rates. The viscosity at the lowest shear rates increases by a factor of 10 during these six days. The reason for this could be the ageing of the system, but in comparison with the clay-water system ageing is not significant.
In the clay-water system, the interaction between particles is electrostatic charges on the edge and face of clay, which during shearing brings about the separation

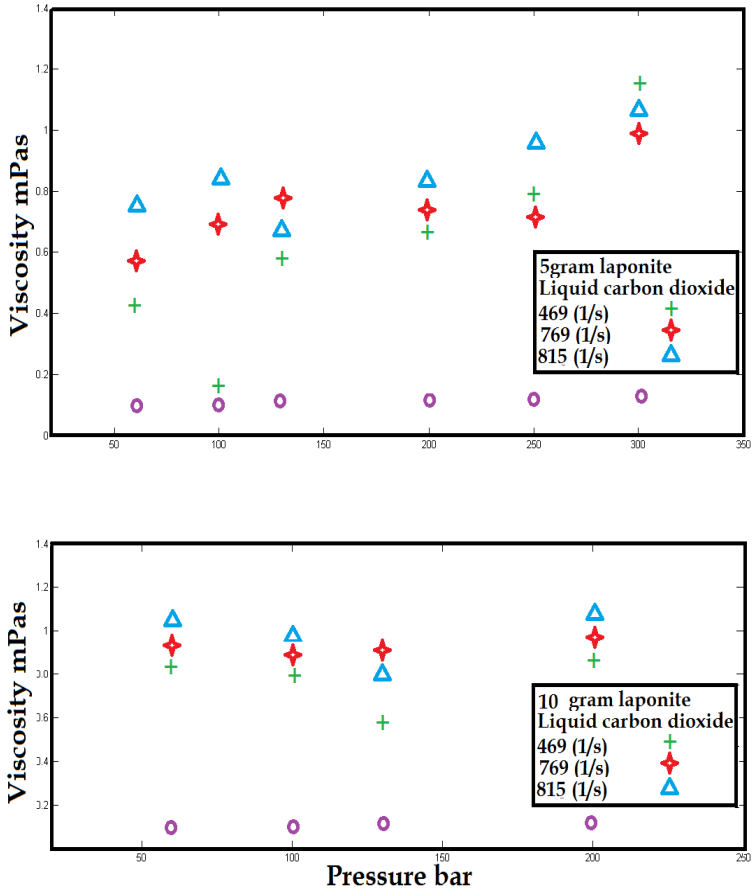

FIGURE 4.20: Viscosity of Laponite versus pressure (a) 5gram Laponite (b) 10gram Laponite. Shear rates 469, 769, 815 (1/s). Temperature 10°C.

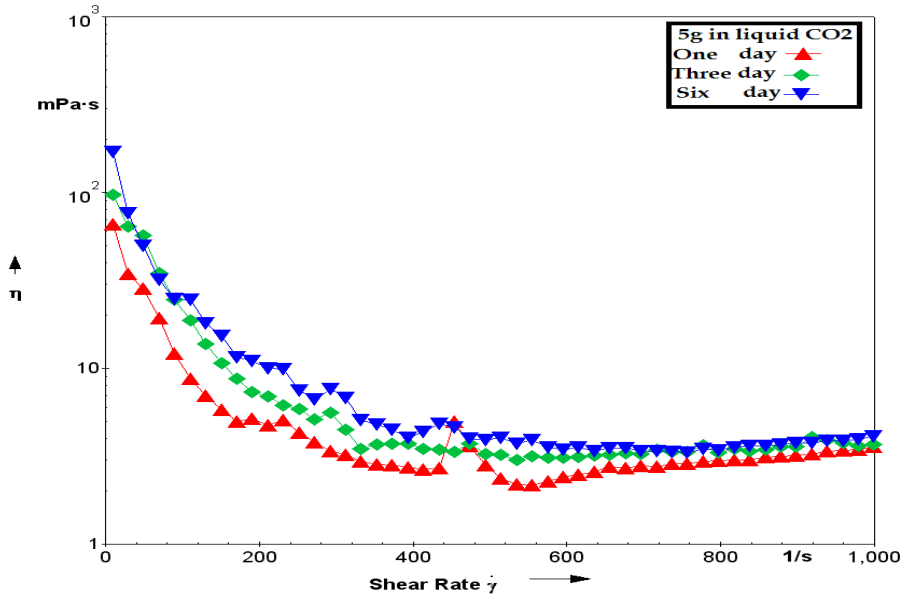

FIGURE 4.21: Viscosity of 5gram laponite particles versus shear rate, during one week.

of the clay into individual clay platelets and forms a house of card like structure. In this work, we stirred the clay in the liquid carbon dioxide which is a non-polar compound which has a very low electrostatic interaction with clays due to London-van der Waals interaction, and it could not interact with clays in the same way as water interacts with hydrogen bonding. For this system viscous forces can also be taken into account, as we know they are proportional to the local velocity difference between the particle and the surrounding fluid which here are clay particles and liquid CO_2 respectively. Consequently the viscosity of the suspension is lower than the clay-water suspension [3, 41].

Chapter 5

Conclusions and suggestions for future studies

Rheology of clay particles suspended in liquid carbon dioxide was performed using two different high pressure systems. In the double gap system clay particles can increase the viscosity of liquid carbon dioxide and this is not dependent on the type of clay. For different types of clay the same rheological behavior was observed. In the Mooney system a higher amount of clay could be added to the cell, so the viscosity of the suspensions was increased in comparison with the double gap system. Non-Newtonian behavior was observed for both systems, which could be due to the interaction of clay particles in the liquid carbon dioxide under flow, or due to the magnetic coupling. A turbulence effect could also occur in a way which affects the measurement of the viscosity. Briefly the viscosity of clay-liquid CO_2 is higher than pure CO_2 and it is shear dependent. A starch pressure cell CC26/PR030 is strongly suggested for future studies. This measurement system would have the capacity to stir the sample and measure rheological behaviors.

Part II

Complex behavior of clay particles in air (Imaging of E-Field induced chain formation from Nano-clays in air)

Chapter 6

Introduction

Field-responsive materials belong to a group of engineering systems, smart materials, whose physical properties strongly depend on the application of an external field upon them. Particularly, electro-active systems, when subjected to high electric fields (of the order of kV/mm), show different behaviors associated to the alteration of their optical (electro-optical effect), electrical, and mechanical properties (electrorheological effect which is the microstructural changes that arise when applying an electric field) [42]. The electrorheological (ER) fluids have been studied for a half century or more and recently have received much attention due to their potential applications in many industrial areas [43]; they could be used in the automotive industrial for clutch, brake, damping systems, robotic arm joints and hands, and military purposes [44]. An example of one of such experiments was conducted by Rozynek,et al [45]. in their experiment the clay particles were suspended in silicone oil or similar oils, making up an electrorheological fluid (ERF). The suspended clay particles are complex fluid and they solidify, or become very viscous, when subjected to an applied electric fluid. The transition from a liquid to a solid like state indicates that an internal ordering of the ER constituents has appeared, leading to dramatic changes in the rheological properties. Application of an electric field induces polarization of the suspended dielectric particles. They

consequently orient in the field and aggregate, which results in the formation of a chain-like structure parallel to the electric field direction. Earlier, the "water" and the electrical double layer were believed to be crucial to the ER effect, since all ER fluids are only active if the dispersed particles adsorb a trace amount of water or surfactants. After the innovation of anhydrous ER fluids in 1985, many scientists felt that the previous knowledge on the mechanism of the ER effect should be substantially modified since either the "water" mechanism or the electrical double layer is unable to give an explanation of the considerably strong ER effect in an ER fluid without any amount of water [43]. The aim of this experiment is to investigate E-field induced structuring from clay particles in the ambient and nitrogen atmosphere by means of optical microscopy and high resolution camera. We want to see that the water is crucial to chain formation by clay particles or they can be formed in dry atmosphere also. Many experiments on clays in oil has been done in Complex matter group at NTNU. This E-field induced chain formation experiment in ambient atmosphere or dry atmosphere is at its infancy. We hope that new students continue this experiment with better set up. Dr. Davi de Miranda Fonseca[1] has done the experiment in glove bag and in Nitrogen atmosphere, and some of his pictures used. The leakage current was tried to measure by using an operational amplifier and a feed back resistance which would be explained.

[1] Pos-doc candidate, NTNU

Chapter 7

Theory

7.1 Electrorheological models

We have already mentioned in the chapter 6 that a polarization is induced in the suspended dielectric particles upon the application an electric field. This polarization was studied with a model based on dielectric constant mismatch between polarized particle and the medium, However it's poor ability to understand ER phenomena, made scientist to introduce conduction model which can be use for situations where the suspension microstructure has been fully formed. Again this model is unable to explain the response time of ER fluid varying from 0.1 ms to 1 s and also it does not reflect the physical essentials of the ER effect. Both Polarization and conduction models are statics one and do not consider the dynamic process occurring in ER fluids. Recent models consider both electric field induced particle aggregation and the interfacial polarization process [43]. Interfacial polarization is usually in hetergenous materials and arise from the accumulation of charge at structural interfaces [46]. Recent models assume dispersed particle and the suspending medium have no intrinsic dielectric dispersion and that the variation of the applied electric field is very slow compared with the rate of polarization are not always valid in the ER fluids case [43]. Figure 7.1 shows optical micro-

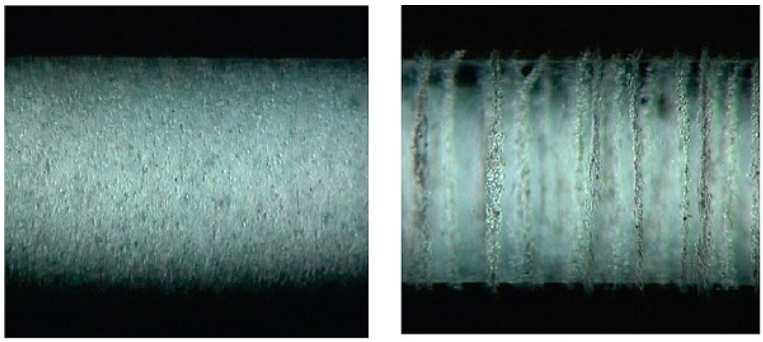

FIGURE 7.1: Suspension of laponite in silicon oil, (a) Static ER fluid under E$\approx$ 0; clay particles are randomly dispersed, (b) Static ER fluid under E 2.0 kV/mm; chain- or column like structures of clay particles have formed [47]

scope images of a laponite/silicone oil suspension placed between electrodes with 2 mm gap when applying 2kV/mm, it is clear the columns of nano clays after 40s in turned field on, the figure shows how the clay particles respond to the field i.e., polarize.

The simplest electro rheological mechanism is the chaining of particles brought about by their polarization in an electric field. In principle, such field-induced chaining should occur whenever there is a mismatch between the bulk dielectric constant of particles, ϵ_p, and that of the suspending medium ϵ_s. Usually

$$\epsilon_r \equiv \epsilon_p/\epsilon_s > 1 \tag{7.1}$$

Particle pairs for which the line separating their centers of mass is parallel to electric field are attracted to each other, while those for which the alignment is perpendicular to the field are mutually repelled. Letting θ be the angle between the field and line joining the centers of two particles, one finds that particles attract each other when θ<55^o; otherwise they repel, see figure 7.2 interactions between

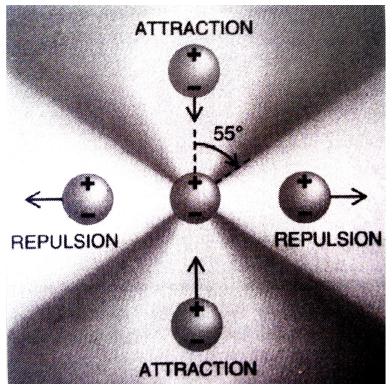

FIGURE 7.2: Interaction between particles polarized by an electric field. Particles whose separation is perpendicular to the field repel each other, while those whose separation is parallel to the field attract [29]

.

particles that are polarized by a vertically oriented electric field illustrated. This mechanism of particle interaction is the basis of the polarization model of ER fluids, which predicts rapid particles chain formation when an electric field is turned on, in agreement with direct visual observations. If the field is maintained, the chains tend to consolidate slowly into thicker columns. Columns of monodisperse particles can eventually organize into a dense phase with body-centered tetragonal symmetry [29].

7.2 The Simple polarization model

The forces which explain ER fluids are *electrostatic*, *hydrodynamic*, and *steric* forces. For small particles, *Brownian* forces might also be present, but since these break up particle structures, it is desirable to use particles big enough($>1\mu$m) to suppress Brownian motion. Ordinarily, particle inertia can be neglected.

Electrostatic Forces In the point-dipole approximation, one assumes that the dipole moment of a particle is not affected by the surrounding particles, and that

the ratio $\epsilon_r \equiv \epsilon_p/\epsilon_s$ is near unity. The dipole moment u of an isolated sphere in a field E is u=$\beta a^3 E$, *where*

$$\beta \equiv \frac{\epsilon_r - 1}{\epsilon_r + 2} \tag{7.2}$$

is the effective polarizability of particle, and a is the particle radius. In the point-dipole approximation, the dipole moments of all particles of a given size are therefore equal and are all aligned parallel to the field. Let θ_{ij} be the angle between the field and the line joining the centers of mass of particles i and j. In the point-dipole approximation, the interaction potential between two particle is

$$W_{e,ij} = -\frac{4\pi\epsilon_0\epsilon_s u^2}{r_{ij}^3}(3\cos^2\theta_{ij} - 1) \tag{7.3}$$

where r_{ij} is the center-of-mass separation between the two particles, $r_{ij} \equiv |\boldsymbol{r}_i - \boldsymbol{r}_j|$, and ϵ_0 is the permittivity of space, $\epsilon_0 = 8.85 \times 10^{-12} C^2 J^{-1} m^{-1}$. The force $F_{ij}^e \equiv -\partial W_{e,ij}/\partial \boldsymbol{r}_i$ on particle *i* produced by particle *j* is then

$$\begin{aligned} F_{ij}^e &= \frac{12\pi\epsilon_0\epsilon_s u^2}{r_{ij}^4}[(3\cos^2\theta_{ij} - 1)\boldsymbol{e}_r^{ij} + \sin 2\theta_{ij}\boldsymbol{e}_\theta^{ij}] \\ &= 12\pi\epsilon_0\epsilon_s\beta^2 a^2 E^2 \left(\frac{a}{r_{ij}^4}\right)^4 [(3\cos^2\theta_{ij} - 1)\boldsymbol{e}_{\boldsymbol{r}}^{\boldsymbol{ij}} + \sin 2\theta_{ij}\boldsymbol{e}_\theta^{ij}] \end{aligned} \tag{7.4}$$

where, again, $u \equiv \beta a^3 E$, $\boldsymbol{r}_j - \boldsymbol{r}_i = r_{ij}\boldsymbol{e}_r^{ij}$, and $\boldsymbol{e}_r^{ij}$ is a unit vector oriented parallel to the line joining the centers of two spheres, while $\boldsymbol{e}_\theta^{ij}$ is a unit vector perpendicular to $\boldsymbol{e}_r^{ij}$ and in the plane containing the field direction (see Fig7.3). Under the point-dipole approximation, the electrostatic forces are pairwise additive, so that the total force $\boldsymbol{F}_i^e$ acting on particle i is given by

$$\boldsymbol{F}_i^e = \sum_{i \neq j} \boldsymbol{F}_{ij}^e \tag{7.5}$$

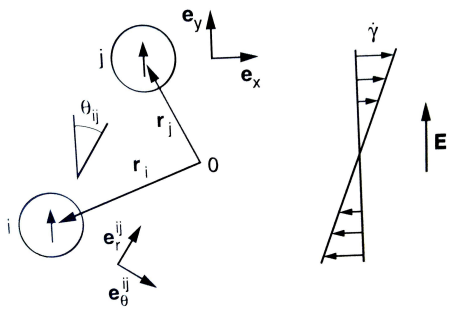

FIGURE 7.3: Coordinate system for a pair of particles in an electric field undergoing a shear deformation[29].

Hydrodynamic Forces The simplest form for hydrodynamic "drag" force $\boldsymbol{F^d}$, namely Stokes drag, is, like the point-dipole approximation, strictly valid only when the particles are widely spaced. In the Stokes-drag approximation, for a shearing flow at shear rate $\dot{\gamma}$, we have

$$\boldsymbol{F}_i^d = -6\pi\eta_s a\left(\frac{d}{dt}\boldsymbol{r}_i - \dot{\gamma}y_i\boldsymbol{e}_x\right) \tag{7.6}$$

where y_i is the coordinate of $\boldsymbol{r}_i$ parallel to the electric field, with $y_i = 0$ on one electrode and $y_i = L$ on the other. The flow direction is x.

Steric Forces A steric repulsive force $\boldsymbol{F}_i^{steric} = \sum_{j\neq i}\boldsymbol{F}_{ij}^{steric}$ must be included to keep particles from overlapping. This steric force would no be required if the hydrodynamic forces were treated more realistically, because as particles approach each other closely, strong lubrication forces are produced by solvent that must be squeezed from between the particles. However, these lubrication forces are omitted from one-particles Stokes' hydrodynamics, and a steric force must be introduced [29].

Brownian Forces Brownian forces can disrupt the particle chains that produce a yield stress, but can be made negligible if the electrostatic forces holding particle

structure together are strong enough, the rate of structural change by Brownian motion could be negligible if particles size were 10 μm or bigger [29].

Chapter 8

Experiment

8.1 Experiment set up

To disperse particles in the air three method were devised. In the first method, a speaker (see figure 8.1) with 18cm diameter was covered with a sheet of paper stuck on the concave surface of the speaker to have a flat surface. The speaker was connected to a signal generator and this speaker disperses the clay particles placed on it into the air. An electrode with 2.5cm length and 2mm gap was used to catch the particles from escaping from the surface of the speaker. The experiment was recorded using a Sony digital Handycam HDR SR12E camera which was connected to the Zeiss Stemi 2000-C microscope with an adapter to record the chain formation on the speaker. The microscope could shift horizontally in order to focus and prevent the particles from settling on the microscope's lens. The sample was poured on the speaker while the electric field in the electrode, suppled by Delta Elektronika ES 030-5 power supply, was connected to a custom high-volt converter which converts a range of 0-15 V into 0-5kV(DC). A signal generator; Tektronix CFG-280 was used to produce an appropriate frequency for the speaker to work. The experimental set up for this method is shown in figure 8.2. The second method consisted of using a "blower"(see figure 8.1(c)) which

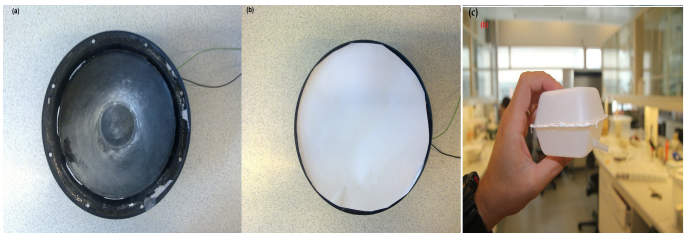

FIGURE 8.1: The speaker (a) without paper (b) paper stuck on it concave surface (c) Blower used instead of speaker to sprinkle or dump particles into the electrode

sprayed a fine stream of clay particles, and the third method consisted in turning the clay container upside down above the electrodes therefore dispensing a large amount of clay powder at once.
A glove bag was prepared in such a way as to provide a nitrogen atmosphere with eventual water molecules being absorbed by desiccant inside it (see figure 8.3). The relative humidity and temperature inside the glove bag were monitored by a Vaisala HMI38 humidity meter, during the experiment it was always under 3%. Every piece of equipment needed was either placed inside the glove bag or close to it with necessary leads going inside the glove bag. The electrode connection was same like without glove bag. Voltage and current were measured with extra gauges, Agilent 34401A and Appa 305 multimeters, respectively. The Petri dishes containing the clay samples were placed in a closed enclosure with desiccant inside which was used to transport them to the glove bag. The glove bag was flushed with nitrogen twice before it was sealed. During the experiment a positive nitrogen pressure was kept in order to ensure that the main gas inside the glove bag was nitrogen. The experiment involved applying an electric field of 450 V/mm and then dispensing clay between the electrodes and trying to observe the formation of chains. The electrode was cleaned with tissues and nitrogen inside the glove bag before using a different clay powder.

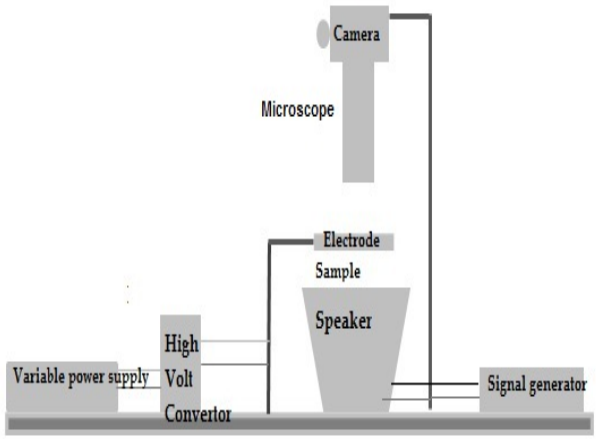

FIGURE 8.2: Experiment set up, while particles was jumping on the speaker, the camera focused on the gap between electrode and chain formation recorded.

8.2 Material

Laponite RD was purchased from Laporte Ltd, USA; and Kaolinite was acquired from Source Clay Minerals Repository, USA. The clay powders were crushed with a mortar and pestle in order to avoid clumps of clay in the studied samples. Some grams of each were poured on the vibrating speaker to jump and some grams were poured into separate Petri dishes, where these placed inside an oven with desiccant for drying at 105 °C for 5 days.

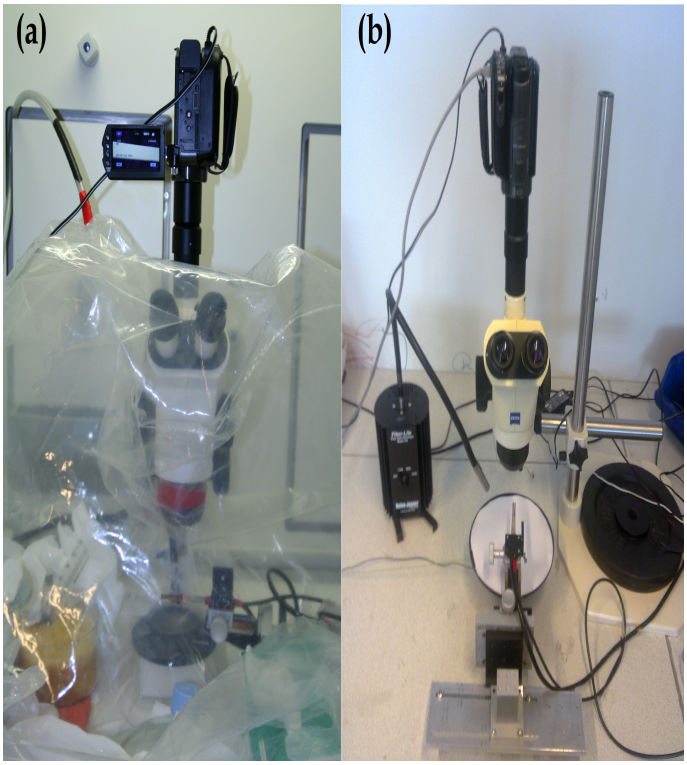

FIGURE 8.3: Imaging of nano-clays chain formation (a) in glove box and dry atmosphere (b) in ambient condition

Chapter 9

Data Analysis and results

9.1 Imaging of clay particles in ambient atmosphere

The chains from clay particles could be formed with voltage ranging from 300 to 1000 V DC. When the voltage is higher than 1000 volt, sparks are observed in the gap. When particles was jumping on speaker, the camera was recording the movement; for laponite and kaolinite this procedure were done, the field which was used in the electrode was 500 V/mm DC. The experiment was first conducted using kaolinite, then laponite. The experiment should have repeated for several times to have a homogeneous particles or a uniform dispersion of clay particles in the air. According to Equation 7.1 there is mismatch between permittivity of nano clays and suspended medium, which here is air. In fact both air and silicon oil are insulators, and the chain formations happen in clays atoms rather than air atoms, so we can probe it. We started with laponite and kaolinite particles and tried to take movies or images of their response to field when they were forming chains. In the figure 9.1 kaolinite particles forms chain in the electrode when the particles are jumping to the air. The time that it takes for these particles to be caught by the electrode was 100 s. The time here is not a characteristic time which would have been the same for each experiment; because we have different initial states and

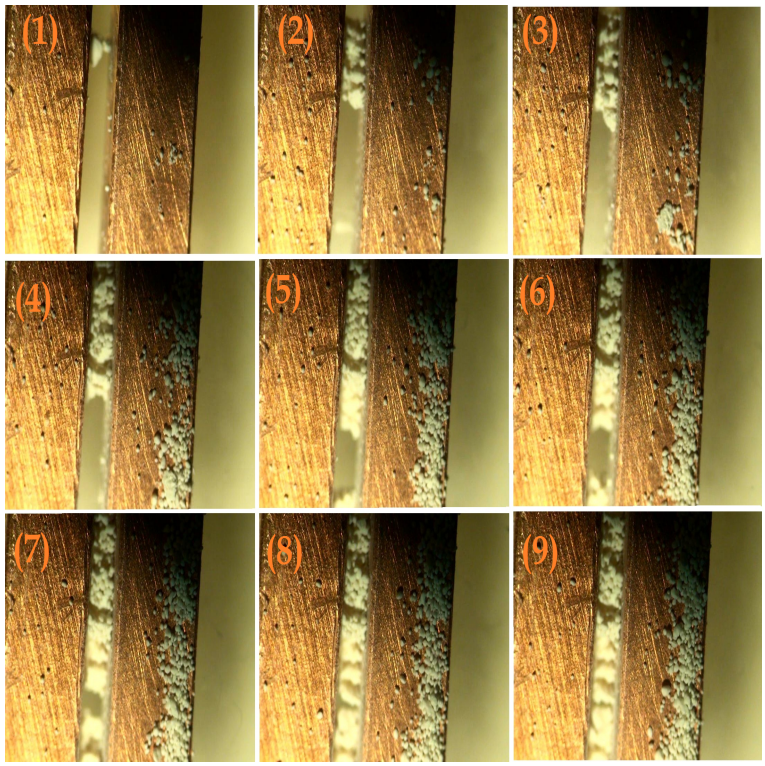

FIGURE 9.1: Kaolinite particles chain formation in the air, applied field to the electrode 500 Volt/mm DC, time 100 s

some times it took more time to see any chain and some time we have very fast, it depend how the speaker could make particles to jump and have homogeneous cloud around the electrode. We should be reminded that the clays particles have not been heated before for this experiment.

In the figure 9.2 laponite particles in the electric field is illustrated, they formed chains very fast almost 5 s. However we can not say the initial condition is the same with kaolinite particles.

Kaolinite particles had bigger particle sizes than laponite and the gap between

FIGURE 9.2: Laponite particles chain formation in the air, applied field 500 V/mm DC, time 5s

electrode was the same, so they could form chain easier than laponite, even when we crushed them several times to have small particles, still laponite particles are smaller and have small size.
In figure 9.3 some individual pictures of the laponite chain formation are shown; it shows the columns parallel to the field when it was on. In figure 9.4 a close up pictures of laponite and kaolinite particles in the electric field are illustrated. one can see the structural formation of both clay particles.
There was chain formation by dumping clay onto electrodes. For doing this, laponite was dried for 2 days at 120°C, transferred from sample preparation laboratory to the experiment place inside a closed dry container (orange silica gel did not change color for days, so inside air was dry and closure was air-tight). Electrode was placed above a hot plate at 250°C; a quick measurement of the air temperature showed that it was above 100°C above the hotplate in the volume of interest. Laponite was dumped onto the electrode and stayed between the electrodes. There was bridge formation and the bridge could withstand moderate physical shock. A strong flick was needed to remove it. The laponite bridge formation is shown in figure 9.5.

FIGURE 9.3: Laponite particles in the electric field when it was on. 500 V/mm DC

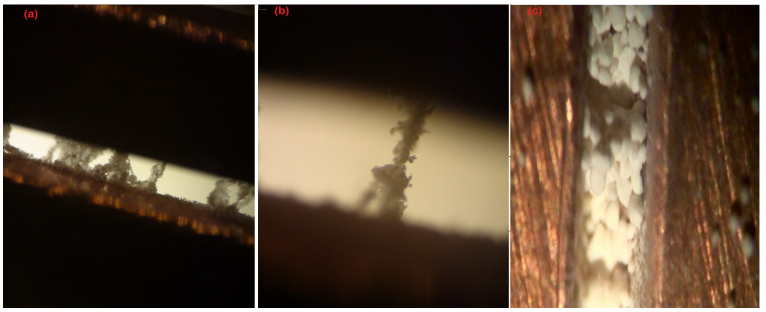

FIGURE 9.4: Clays particles in the air (a,b) laponite particles (c) Kaolinite particles

FIGURE 9.5: Laponite bridge formation

9.2 Imaging of clay particles in Nitrogen atmosphere

The set up was taken inside the glove bag except speaker. In figure 9.6 kaolinite particles are shown when the field is on and the particles are sticking to the electrodes. Figure 9.7 shows kaolinite particles before turning off the field and one can see after one day that they still stayed between the gap, the same observation was made in the case of the laponite. Figure 9.8 shows laponite particles when the field was on and after one day, they stayed between the gap.

9.3 Discussion

When colloid suspension of nano-clays in insulating fluid (Silicon oil) is subjected to an external field, they forms chains and columns parallel to applied electric field. The orientation is explained by interaction of induced electric dipoles, since only particles with suitable polarization properties align into chain formations. The dipolar chain formation is character of ER fluids. It is not only polarization which make the colloid a good ER fluid, but also the property which allows them to rotate under electric field; they are electrically anisotropic and their interfacial polarizability is important. Nano-clays like laponite or kaolinite which have platelet particles, polarize along their silica sheets. Their intercalated cations

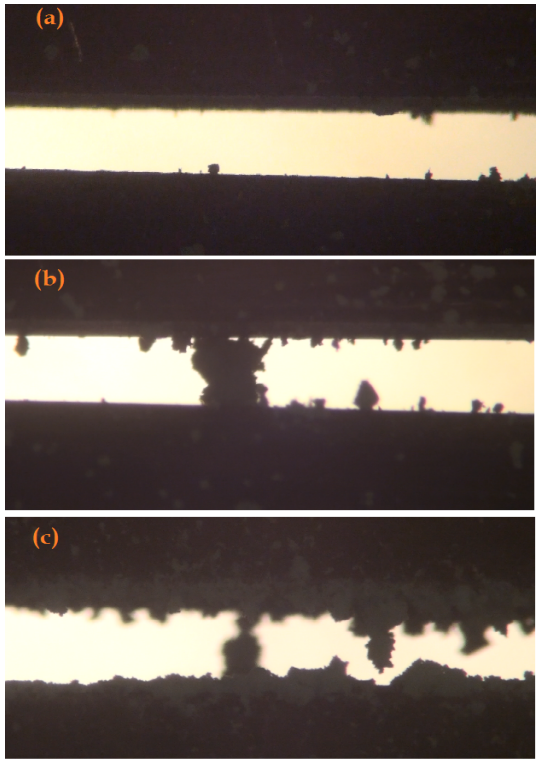

FIGURE 9.6: Kaolinite particle (a) sticking to electrodes when field is on, (b) and (c) kaolinite chain

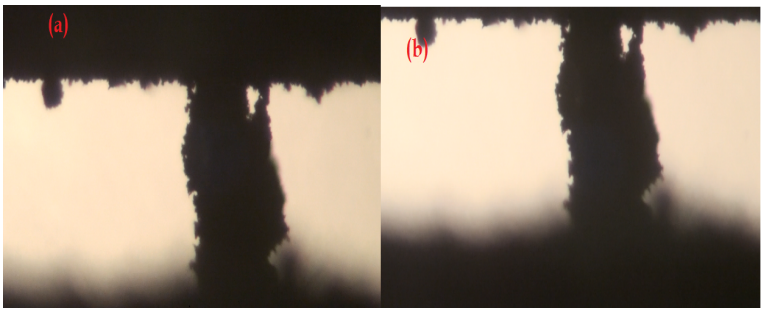

FIGURE 9.7: Kaolinite particle in electric field (a) just before turning the field off and (b) turned field off next day

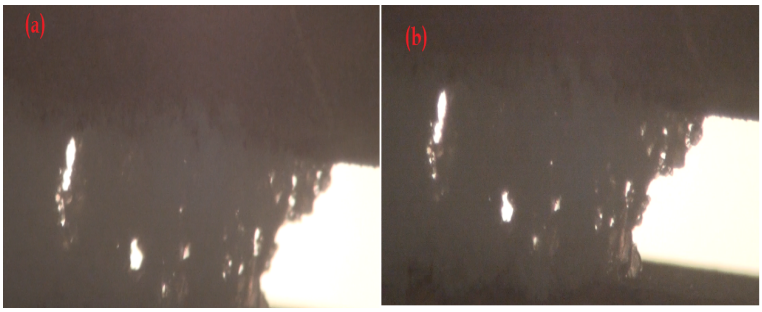

FIGURE 9.8: Laponite particle bridge (a) turned the field on (b) turned the field off

and water between layers has the main role in the interfacial polarization. Clays belong to two groups 2:1 and 1:1 shows different ER effect. Smectite clay (2:1) like Na-fluorohectorite forms chain better than 1:1 type clays in terms of order. Kaolinite (1:1) suspensions appeared much less ordered than those observed in the smectites or 2:1 clays [48]. In this experiment clays were not suspended in oil, they are in air and can form structure when there is no water intercalated between layers. It therefore means that the interfacial polarization is due to intercalated cations rather than water. In the chain formation with electrode on the speaker, it was generally easy to make chain by clay particles. We just needed a uniform cloud of particles to form chain, but it happened sometimes that particles escaped from the electrode. Laponite did not form chains when the blower was employed in order to dispense fine streams of clay between the electrodes; and Kaolin started forming chains right away. Indeed laponite particles did not even stay on top of the electrodes whereas Kaolinite particles could be found everywhere on the surface of the electrodes. Another part of the experiment was observing what happened when a substantial amount of clay powder was dumped onto the electrodes. Employing this method revealed that both laponite and Kaoliinte formed chains connecting the electrodes. It is worth mentioning that all the observed chains were persistent, i.e. even after the electric field was switched off the chains were still present. In fact, a moderate physical shock was necessary in order to remove them. The chains proved to remain many hours (> 12 hours) after the field was turned off; however no attempt was made to determine for how long. Since part of the explanation of the chain formation attributes an important role to the water molecules inside the clay particles, one could suggest that the precautions taken to avoid the presence of water molecules inside the glove bag were not enough. Indeed, after performing the experiment, a number of improvements in setup were devised, such as using a better grade nitrogen gas. However the fact that the laponite particles did not stick to the electrodes strongly points that the clay was dry.

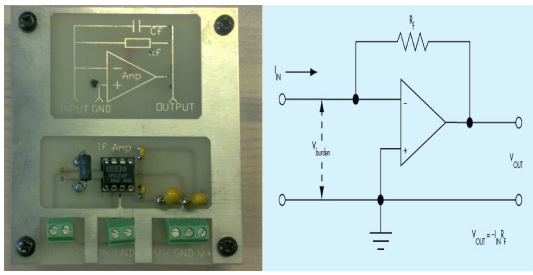

FIGURE 9.9: The feedback ammeter circuit injects the current to be measured directly to the summing junction of the op amp. The output is a voltage proportional to the current that is measure on a Digital multi meter [49].

9.3.1 The current measurement

During the experiment the current was probed as a way of trying to explain the observations, however the measurements were inconsistent; the current oscillated between 1 and 9 μA independent of changes being made. Consequently, unfortunately nothing can be concluded from the current measurement by a multimeter, so an operational amplifier (Op-Amp) and a feedback resistor $\mathrm{R_F}$ were used to measure the current between electrode when chains had formed. This method is for measuring very low current and we expected such low current to measure. As shown in figure 9.9 the output voltage is measured and divide by feedback resistance and the result is the current in the burden or Nano-clay particle chains in this case. According to kirchhoffs law, the current in the feedback resistance and burden is the same so we can write $\mathrm{V_{OUT}} = -\mathrm{I_{IN}R_F}$; $\mathrm{I_{IN}}$ is the current that we intended to measure and the $\mathrm{V_{OUT}}$ is out voltage which is measured by a voltmeter. When $\mathrm{V_{OUT}}$ is divided by $\mathrm{R_F}$ we obtain the desired current. It is clear that the current in the resistor is in the opposite direction to the electrode resistance according to Kirchhoffs circuit laws [49]. To test the circuit a big resistance 1.5G Ω was used instead of the electrode; a big resistance was chosen to be sure that the circuit could measure low currents.

The ultra low bias current of the operational amplifier was 10pA which means currents less than this was not measurable. The currents around a nA could be measured with 1.5GΩ resistance. The operational amplifier was working with ± 15 Volt hence it was not possible to get an output voltage greater than this so for controlling the output voltage the feed back resistance had to be adjusted to have a voltage between 0-15 V. For doing this, different range of resistors were examined from 10 kΩ to 800 MΩ; the appropriate feedback resistance 100 MΩ. When the electrode was full with the chains and electric field was on. Current measured with this method is again not reliable because it was oscillated between 10^{-6} and 10^{-7} A. Therefore we can conclude that the leakage current in the electrode is not in the range nA. We could not increase the voltage because it caused the spark in the gap. The measurement of current was therefore very difficult and we may have just measured some noises. because the area of $0.2 \times 2.5cm^2 = 0.5cm^2$, even when the clay columns filled the gap in the electrode the current was not not stable. When the experiment was repeated with kaolinite particles wetted with water, we could measure significant current even with the multimeter. This is shown in figure 9.10. We can therefore conclude that water increases the current between electrode. We can also observe from figure 9.10 that the begin to fall off with time after approximately 42 s. This can be attributed to the drying of the clay particles. However it is difficult to find explanation for this behavior of the current.

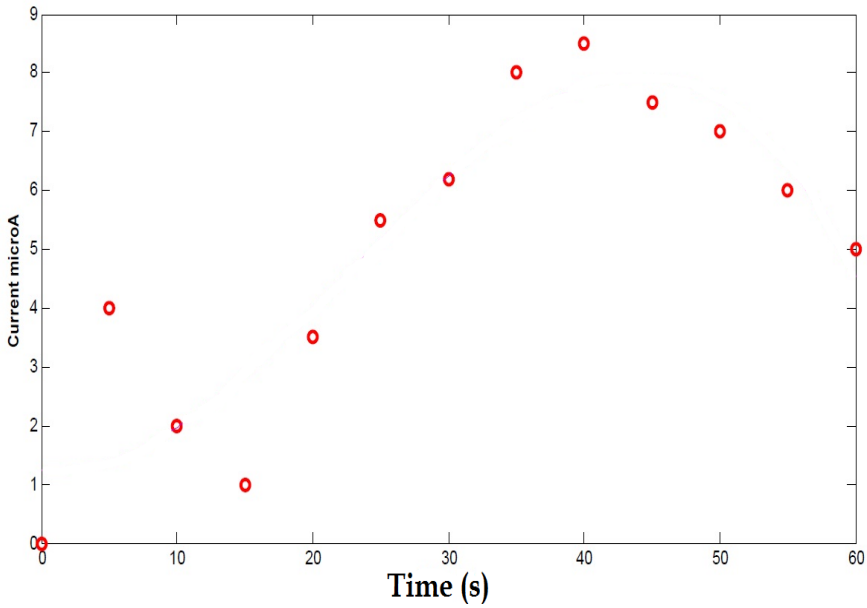

FIGURE 9.10: Kaolinite partilcles current leakage between gap when the field was on, they wet a little before forming chain

Chapter 10

Conclusions and suggestions for future studies

An electrical field was used to induce nano-clay particles to form chains in an ambient and a Nitrogen atmosphere. The effect of hydrous and anhydrous situations on chain formation was observed. It seemed that in both situations chain formation takes place and is not dependent to the humidity of the environment. However it could be that the level of dryness in the glove bag was not adequate, so the chain formation could be due to humidity in the clay particles. One suggestion for improving the result is to dry the clay in an oven and insert it into a capillary tube and close off the entrance and place it in the electrical field to observe how the clay particles behave. Nevertheless, to be more conclusive more experiments are needed.

List of Figures

2.1 (a) Tetrahedron (b) Octahadron [5]. 6
2.2 Silicate building blocks [4]. 7
2.3 Up:1:l(T:O) Kaolinite and Down 2:l (T:O:T) muscovite [4]. 8
2.4 Idealised structural formula of Laponite [8]. 9
2.5 Na-Fluorohectorite with T:O:T structure, Na^+ is intercalated cation [13]. 11
2.6 Phase diagram for carbon dioxide [17]. 13
2.7 A chamber containing two phases of carbon dioxide–liquid and gas. As temperature and pressure increase (from left to right), the two phases merge to become a supercritical fluid [19] 14
2.8 Particle motion in shear and extensional flow [21]. 14
2.9 Left tensile stress and right shear stress [22] 16
2.10 A velocity gradient produced when a fluid is sheared [22]. 17
2.11 Concentric cylinder (a) double gap (b) Mooney 21

3.1 Experimental set up including high pressure cell, syringe pump and CO_2 bottle 26
3.2 The rheometer uses magnetic coupling to transfer torque from instrument motor to the pressure cell. (a) Magnetic coupling (b) The high pressure cell mounted in the Physica MCR 300 (c) Pressure cup and Head with Mooney geometry 27
3.3 Coaxial cylinder measuring system CC33.2/PR [34]. 28

3.4 Double gap concentric cylinder measuring geometry DG35.12/PR [34]. 29
3.5 (a) Pt100 cable for reading the temperature (b) pressure sensor for measuring pressure. 30
3.6 Pressure head and ball bearing located inside of the head [34]. . . 31
3.7 TELEDYNE ISCO Syringe Pump 260D 32

4.1 Good ball bearing check 36
4.2 The viscosity as a function of time for the double gap high pressure cell containing distilled water at ambient atmosphere., sheared at constant shear stress 1.04, 1.25 and 1.46 Pa. The correct viscosity for distilled water is about 1 mPas. 37
4.3 The viscosity as a function of time for the double gap high pressure cell containing Silicon oil Dow Corning 200/10cS at ambient atmosphere, sheared at constant shear rate 1000, 1500 and 2000 1/s. The correct viscosity of silicon oil 200/10cS is 10mPas. . . . 38
4.4 liquid carbon dioxide in 60bar and 10c (a) viscosity versus shear rate 100 to 2400 1/s (b) viscosity versus time. Applied Shear stress 0.2 Pa 39
4.5 Viscosity as a function shear stress for different type of clay, Na-Fluorhectorite, Quick clay, Na-Montmorillite and Laponite in pressure 60 bar and temperature 10 °C. 40
4.6 Flow curve for four different type of clays, including Na-Fluorhectorite, Quick clay, Na-Montmorillite and Laponite. Pressure 60 bar and temperature 10 °C. 41
4.7 Viscosity behavior 0.3gram laponite and liquid CO_2. Shear rate applied 1000, 2000, 3000 (1/s). Pressure 60 bar and temperature 10°C. 42
4.8 Viscosity behavior 0.3gram Quick clay in the liquid CO_2 versus time. Shear rate applied 1000, 2000 and 3000 (1/s). Pressure 60 bar and temperature 10 °C. 43

4.9 Variation of viscosity with shear stress with different pressure from 60bar to 300bar, temperature 10°C 44
4.10 The viscosity as a function of time for the Mooney high pressure cell containing distilled water at ambient atmosphere, sheared at constant shear stress 1.3, 2.26 and 3.39 Pa. The correct viscosity for distilled water is about 1 mPas. 46
4.11 The viscosity as a function of time for the Mooney high pressure cell containing distilled Silicon oil Dow corning 200/10cS at ambient atmosphere, sheared at constant shear stress 2.2, 4.5 and 6.7 Pa. The correct viscosity of silicon oil 200/10cS is 10 mPas. . . . 47
4.12 Viscosity of 3gram Quick clay and flow curve in different pressure. (a) viscosity vs shear stress (b) shear rate vs shear stress. Pressure 60, 70, 80, 100 and 120 bar and temperature 10 °C. . . . 49
4.13 (a) Viscosity of 5gram Quick clay and flow curve in different pressure (a) Viscosity versus shear stress (b) Shear rate versus shear stress. Pressure 60, 100, 130 and 200 bar and temperature 10°C. . 50
4.14 Viscosity of 5g laponite and liquid carbon dioxide. (a) viscosity vs shear rate (b) flow curve. Pressure 60, 100, 200 and 300 bar and temperature 10°C. 51
4.15 Viscosity of 10g laponite and carbon dioxide. (a) viscosity vs shear rate (b) shear stress vs shear rate. bar. Applied shear rate 100 to 1000(1/s). Pressure 60, 100, 130 and 200 and temperature 10 °C. 52
4.16 The viscosity coefficient of carbon dioxide as a function of pressure, open symbols: in the stable state, filled symbol: in the metastable state. △ 220K, Diamond 230K, ▽ 240K, ○ 260K, Box 280K, × 300K, ⋆ 303K, + 308K. From [37]. 53
4.17 Viscosity of carbon dioxide in pressure range 40 to 320 bar, temperature 280 K. Data from [37]. 54

4.18 Viscosity as a function of pressure. 0.3 gram laponite in the Double gap system. Shear stress 1 Pa, 2.5 Pa and 4 Pa. 56
4.19 Viscosity of Quick clay versus pressure in different shear stress. (a) 3gram Quick clay in 2.5, 5.5 and 7.5 Pa shear stress. (b) 5gram Quick clay in 0.6 and 1.03 Pa. Temperature 10°C. 58
4.20 Viscosity of Laponite versus pressure (a) 5gram Laponite (b) 10gram Laponite. Shear rates 469, 769, 815 (1/s). Temperature 10°C. . . . 60
4.21 Viscosity of 5gram laponite particles versus shear rate, during one week. 61

7.1 Suspension of laponite in silicon oil, (a) Static ER fluid under E≈ 0; clay particles are randomly dispersed, (b) Static ER fluid under E 2.0 kV/mm; chain- or column like structures of clay particles have formed [47] 70
7.2 Interaction between particles polarized by an electric field. Particles whose separation is perpendicular to the field repel each other, while those whose separation is parallel to the field attract [29] . . 71
7.3 Coordinate system for a pair of particles in an electric field undergoing a shear deformation[29]. 73

8.1 The speaker (a) without paper (b) paper stuck on it concave surface (c) Blower used instead of speaker to sprinkle or dump particles into the electrode 76
8.2 Experiment set up, while particles was jumping on the speaker, the camera focused on the gap between electrode and chain formation recorded. 77
8.3 Imaging of nano-clays chain formation (a) in glove box and dry atmosphere (b) in ambient condition 78

9.1 Kaolinite particles chain formation in the air, applied field to the electrode 500 Volt/mm DC, time 100 s 80

9.2 Laponite particles chain formation in the air, applied field 500 V/mm DC, time 5s 81
9.3 Laponite particles in the electric field when it was on. 500 V/mm DC 82
9.4 Clays particles in the air (a,b) laponite particles (c) Kaolinite particles 82
9.5 Laponite bridge formation 83
9.6 Kaolinite particle (a) sticking to electrodes when field is on, (b) and (c) kaolinite chain 84
9.7 Kaolinite particle in electric field (a) just before turning the field off and (b) turned field off next day 85
9.8 Laponite particle bridge (a) turned the field on (b) turned the field off 85
9.9 The feedback ammeter circuit injects the current to be measured directly to the summing junction of the op amp. The output is a voltage proportional to the current that is measure on a Digital multi meter [49]. 87
9.10 Kaolinite partilcles current leakage between gap when the field was on, they wet a little before forming chain 89

References

[1] A. Botan, B. Rotenberg, V. Marry, P. Turq, and B. Noetinger. Carbon dioxide in montmorillonite clay hydrates: Thermodynamics, structure, and transport from molecular simulation. *The Journal of Physical Chemistry C*.

[2] J.M. Nordbotten, M.A. Celia, and S. Bachu. Injection and storage of co 2 in deep saline aquifers: Analytical solution for co 2 plume evolution during injection. *Transport in Porous Media*, 58(3):339–360, 2005.

[3] H.A. Barnes, J.F. Hutton, and K. Walters. *An introduction to rheology*. Elsevier, 1998. ISBN 044487469.

[4] RH White, MA Dietenberger, KHJ Buschow, RW Cahn, MC Flemings, B. Ilschner, EJ Kramer, and S. Mahajan. Encyclopedia of materials: science and technology. *Encyclopedia of materials: science and technology*, 2001.

[5] P.A. Ciullo. *Industrial minerals and their uses: a handbook and formulary*. William Andrew, 1996. ISBN 0815514085.

[6] A. Bakk, J.O. Fossum, G.J. da Silva, H.M. Adland, A. Mikkelsen, and A. Elgsaeter. Viscosity and transient electric birefringence study of clay colloidal aggregation. *Physical Review E*, 65(2):021407, 2002.

[7] D.B. Braun and M.R. Rosen. *Rheology modifiers handbook: practical use and application*. William Andrew, 2000.

[8] Rockwood Additives Ltd. Laponite – Performance additives. `http://www.scprod.com/pdfs/LaponiteBrochureE.pdf`, 2007.

[9] L.A. Utracki. *Clay-containing polymeric nanocomposites*, volume 1. Smithers Rapra Technology, 2004.

[10] F. Bossard, M. Moan, and T. Aubry. Linear and nonlinear viscoelastic behavior of very concentrated plate-like kaolin suspensions. *Journal of Rheology*, 51:1253, 2007.

[11] N. I. Ringdal, D. M. Fonseca, E. L. Hansen, H. Hemmen, and J. O. Fossum. Nematic textures in colloidal dispersions of na-fluorohectorite synthetic clay. *Phys. Rev. E*, 81(4):041702, Apr 2010. doi: 10.1103/PhysRevE.81.041702.

[12] E. DiMasi, JO Fossum, T. Gog, and C. Venkataraman. Orientational order in gravity dispersed clay colloids: A synchrotron x-ray scattering study of na fluorohectorite suspensions. *Physical review E*, 64(6):061704, 2001.

[13] H. Hemmen, N.I. Ringdal, E.N. De Azevedo, M. Engelsberg, E.L. Hansen, Y. Met'heust, J.O. Fossum, and K.D. Knudsen. The isotropic- nematic interface in suspensions of na- fluorohectorite synthetic clay. *Langmuir*, 25(21): 12507–12515, 2009.

[14] M. Segad, B. Jonsson, T. Åkesson, and B. Cabane. Ca/na montmorillonite: Structure, forces and swelling properties. *Langmuir*, 26(8):5782–5790, 2010.

[15] A. Khaldoun, P. Moller, A. Fall, G. Wegdam, B. De Leeuw, Y. Méheust, J. Otto Fossum, and D. Bonn. Quick clay and landslides of clayey soils. *Physical review letters*, 103(18):188301, 2009.

[16] P. Patnaik and Knovel (Firm). *Handbook of inorganic chemicals*. McGraw-Hill New York, 2003. ISBN 0070494398.

[17] W. Leitner. Green chemistry: Designed to dissolve. *Nature a-z index*, 405 (6783):129–130, 2000.

[18] P.A. Carson, C.J. Mumford, and Knovel (Firm). *Hazardous chemicals handbook*. Butterworth-Heinemann, 2002. ISBN 0750648880.

[19] T Miller, K. Phillips. Harvesting mars. `http://www.nasa.gov/vision/earth/technologies/harvestingmars.html`, March 2007.

[20] A. Gupta. *Feasibility of supercritical carbon dioxide as a drilling fluid for deep underbalanced drilling operations*. PhD thesis, Louisiana State University, 2006.

[21] H.A. Barnes, Institute of Non-Newtonian, and Fluid Mechanics. *A handbook of elementary rheology*. University of Wales, Institute of Non-Newtonian Fluid Mechanics, 2000. ISBN 0953803201.

[22] J.W. Goodwin, J.W. Goodwin, and R.W. Hughes. *Rheology for chemists: an introduction*. RSC Publishing, 2000. ISBN 085404616.

[23] S.S. Bair. *High-pressure rheology for quantitative elastohydrodynamics*. Elsevier Science, 2007. ISBN 0444522433.

[24] Stuart Craig. Anton paar: Pressure cells for simultaneous rheological testing. `http://www.mep.net.au/press/release/M123_Pressure_cells_MEP.pdf`, march 2007.

[25] S. Rossi, P. Luckham, S. Zhu, and B. Briscoe. High-pressure/high-temperature rheology of Na+-montmorillonite clay suspensions. In *SPE International Symposium on Oilfield Chemistry*, 1999.

[26] C.W. Macosko and R.G. Larson. *Rheology: principles, measurements, and applications*. Wiley-Vch, 1994. ISBN 0471185752.

[27] NMB Flichy, CJ Lawrence, and SG Kazarian. Rheology of poly (propylene glycol) and suspensions of fumed silica in poly (propylene glycol) under high-pressure CO2. *Industrial & engineering chemistry research*, 42(25): 6310–6319, 2003. ISSN 0888-5885.

[28] J.R. Royer, Y.J. Gay, M. Adam, J.M. DeSimone, and S.A. Khan. Polymer melt rheology with high-pressure CO2 using a novel magnetically levitated sphere rheometer. *Polymer*, 43(8):2375–2383, 2002. ISSN 0032-3861.

[29] R.G. Larson. The structure and rheology of complex fluids. *New York: Oxford*, 2001.

[30] Anton Paar. Physica mcr, the modular rheometer series. `http://www.oleinitec.fi/pdf/Physica/mcr_serie_e.pdf`, 2002.

[31] M.J. Wingert, S. Shukla, K.W. Koelling, D.L. Tomasko, and L.J. Lee. Shear Viscosity of CO2-Plasticized Polystyrene Under High Static Pressures. *Industrial & Engineering Chemistry Research*, 48(11):5460–5471, 2009. ISSN 0888-5885.

[32] *Instruction Manual pressure cell 400bar*. Antoon Paar, Paar GmbH, Anton-Paar-Str.20, A-8054 Graz/Austria-Europe, March 2007.

[33] A. Heritage. A basic introduction to rheology. *Bohlin Reference: BIR-V1. 0, Bohlin Instruments Ltd. Gloschestershire, UK: The Corinium Center at Cirencester. p*, pages 1–13, 1994.

[34] Hubert Reitberger. Pressure cell different requirements different versions, 2005.

[35] T.G. Mezger. *The rheology handbook: for users of rotational and oscillatory rheometers*. Vincentz Network GmbH & Co KG, 2006. ISBN 3878701748.

[36] *D-series Pump, Installation and Operation Guide*. TELEDYNE ISCO, February 2010.

[37] PS Van Der Gulik. Viscosity of carbon dioxide in the liquid phase. *Physica A: Statistical and Theoretical Physics*, 238(1-4):81–112, 1997.

[38] J.R. Royer, Y.J. Gay, J.M. Desimone, and S.A. Khan. High-pressure rheology of polystyrene melts plasticized with co2: Experimental measurement and predictive scaling relationships. *Journal of Polymer Science Part B: Polymer Physics*, 38(23):3168–3180, 2000.

[39] A. Amiri, G. Řye, and J. Sj
"oblom. Temperature and pressure effects on stability and gelation properties of silica suspensions. *Colloids and Surfaces A: Physicochemical and Engineering Aspects*, 2011. ISSN 0927-7757.

[40] NMB Flichy, CJ Lawrence, and SG Kazarian. Combining rheology and spectroscopy for studying of polymeric materials subjected to high-pressure carbon dioxide. 2000.

[41] D. Bonn, P. Coussot, HT Huynh, F. Bertrand, and G. Debrégeas. Rheology of soft glassy materials. *EPL (Europhysics Letters)*, 59:786, 2002.

[42] MJ Espin, AV Delgado, and J. Plocharski. Quasi-static electrorheological properties of hematite/silicone oil suspensions under dc electric fields. *Langmuir*, 21(11):4896–4903, 2005.

[43] T. Hao, A. Kawai, and F. Ikazaki. Mechanism of the electrorheological effect: evidence from the conductive, dielectric, and surface characteristics of water-free electrorheological fluids. *Langmuir*, 14(5):1256–1262, 1998.

[44] T. Hao. Electrorheological suspensions. *Advances in colloid and interface science*, 97(1-3):1–35, 2002.

[45] Z. Rozynek, KD Knudsen, JO Fossum, Y. Méheust, B. Wang, and M. Zhou. Electric field induced structuring in clay–oil suspensions: new insights from waxs, sem, leak current, dielectric permittivity, and rheometry. *Journal of Physics: Condensed Matter*, 22:324104, 2010.

[46] C. Kittel and P. McEuen. *Introduction to solid state physics*. Wiley New York, 1986.

[47] KPS Parmar, Y. Meheust, B. Schjelderupsen, and JO Fossum. Electrorheological suspensions of laponite in oil: rheometry studies. *Langmuir*, 24(5): 1814–1822, 2008.

[48] JO Fossum, Y. Méheust, KPS Parmar, KD Knudsen, KJ Måløy, and D.M. Fonseca. Intercalation-enhanced electric polarization and chain formation of nano-layered particles. *EPL (Europhysics Letters)*, 74:438, 2006.

[49] LE Frenzel. Basics of design accurately measure nanoampere and picoampere currents. *ELECTRONIC DESIGN-NEW YORK THEN HASBROUCK HEIGHTS THEN CLEVELAND OH-*, 55(4):32, 2007.